Reproducibility of sound-absorbing periodic porous materials using additive manufacturing technologies: Round robin study

Tomasz Zieliński, Kamil Opiela, Piotr Pawlowski, Nicolas Dauchez, Thomas Boutin, John Kennedy, Daniel Trimble, Henry Rice, Bart van Damme, Gwenael Hannema, et al.

▶ **To cite this version:**

Tomasz Zieliński, Kamil Opiela, Piotr Pawlowski, Nicolas Dauchez, Thomas Boutin, et al.. Reproducibility of sound-absorbing periodic porous materials using additive manufacturing technologies: Round robin study. Additive Manufacturing, 2020, 36, pp.101564. 10.1016/j.addma.2020.101564 . hal-03084698

HAL Id: hal-03084698
https://hal.science/hal-03084698v1

Submitted on 21 Dec 2020

HAL is a multi-disciplinary open access archive for the deposit and dissemination of scientific research documents, whether they are published or not. The documents may come from teaching and research institutions in France or abroad, or from public or private research centers.

L'archive ouverte pluridisciplinaire **HAL**, est destinée au dépôt et à la diffusion de documents scientifiques de niveau recherche, publiés ou non, émanant des établissements d'enseignement et de recherche français ou étrangers, des laboratoires publics ou privés.

Manuscript File Click here to view linked References

Reproducibility of sound-absorbing periodic porous materials using additive manufacturing technologies: Round robin study

Tomasz G. Zieliński[a,*], Kamil C. Opiela[a], Piotr Pawłowski[a], Nicolas Dauchez[b], Thomas Boutin[b], John Kennedy[c], Daniel Trimble[c], Henry Rice[c], Bart Van Damme[d], Gwenael Hannema[d], Rafał Wróbel[e], Seok Kim[f], Shahrzad Ghaffari Mosanenzadeh[f], Nicholas X. Fang[f], Jieun Yang[g], Baltazar Briere de la Hosseraye[g], Maarten C. J. Hornikx[g], Edouard Salze[h], Marie-Annick Galland[h], René Boonen[i], Augusto Carvalho de Sousa[i,j], Elke Deckers[i,j], Mathieu Gaborit[k,l], Jean-Philippe Groby[l]

[a] *Institute of Fundamental Technological Research, Polish Academy of Sciences, ul. Pawińskiego 5B, 02-106 Warsaw, Poland*
[b] *Université de Technologie de Compiègne, Alliance Sorbonne Université, CNRS FRE 2012, Laboratoire Roberval, Centre de recherche Royallieu, CS 60319, 60203 Compiègne CEDEX, France*
[c] *Trinity College Dublin, Department of Mechanical & Manufacturing Engineering, Dublin 2, Ireland*
[d] *Swiss Federal Laboratories for Materials Science and Technology, Laboratory for Acoustics/Noise Control, Überlandstrasse 129, 8600 Dübendorf, Switzerland*
[e] *Swiss Federal Laboratories for Materials Science and Technology, Advanced Materials Processing, Überlandstrasse 129, 8600 Dübendorf, Switzerland*
[f] *Massachusetts Institute of Technology, Department of Mechanical Engineering, 77 Massachusetts Avenue, Cambridge, Massachusetts, USA*
[g] *Eindhoven University of Technology, Department of the Built Environment, P.O. Box 513, 5600 MB Eindhoven, the Netherlands*
[h] *Ecole Centrale de Lyon, Université de Lyon, CNRS UMR 5509, Laboratoire de Mécanique des Fluides et d'Acoustique, 36 avenue Guy de Collongue, 69134 Écully CEDEX, France*
[i] *KU Leuven, Department of Mechanical Engineering, Celestijnenlaan 300B box 2420, 3001 Heverlee, Belgium*
[j] *DMMS-D Lab, Flanders Make, Belgium*
[k] *KTH Royal Institute of Technology, Department of Aeronautical and Vehicle Engineering, SE-100 44 Stockholm, Sweden*
[l] *Laboratoire d'Acoustique de l'Université du Mans, LAUM – UMR CNRS 6613, Le Mans Université, Avenue Olivier Messiaen, 72085 LE MANS CEDEX 9, France*

Abstract

The purpose of this work is to compare the acoustic properties (in particular, sound absorption) for samples manufactured using various Additive Manufacturing (AM) technologies. The work is a round robin test (inter-laboratory test), in which the production of samples (with the same agreed periodic microstructure) and their acoustic measurements are carried out independently by different laboratories. Most important, however, is that different additive manufacturing technologies (and different types of equipment) are used to make samples. It was found that this is the main but not the only reason for the discrepancy between the results of acoustic measurements obtained for different porous samples based on the same design of periodic micro-geometry.

Key words: Porous materials, Designed periodicity, Additive manufacturing, Sound absorption

*Corresponding author.
Email address: tzielins@ippt.pan.pl (Tomasz G. Zieliński)

1. Introduction

Although standard porous materials, like open cell foams or fibrous material, are still very competitive for acoustic treatments, their efficiency is limited in the low frequency range by their thickness [1]. If their microstructure can be optimized to meet specific requirements [2–4], their manufacturing is now achievable using 3D printing techniques for experimental validation at the scale of a laboratory. Indeed, the development of Additive Manufacturing (AM) technologies [5–12] give new possibilities to manufacture and test optimised micro-geometries. Moreover, new acoustic materials (or their prototypes) are already being developed using AM technologies, e.g.: 3D-printed periodic foams [13], optimally graded porous materials [2], adaptable sound absorbers [14], acoustic metamaterials based on the Kelvin cell [15], periodic acoustic structures composed of rigid micro-rods [16] or micro-bars [17], and even micro-perforated panels [18, 19] and plates with complex patterns of micro-slits [20]. Most of this research indicates great potential for the development of new acoustic materials using AM technology. However, 3D-printing technology should be evaluated regarding the quality of the reproduced micro-geometry and its influence on sound dissipation. The purpose of this work is to evaluate the influence of several additive manufacturing technologies on the sound absorption of 3D printed samples. Following well-established traditions in acoustic [21, 22] and non-acoustic [23–25] testing of materials, this work is a round robin test, i.e. an inter-laboratory test, where manufacturing of samples and their acoustical measurements are performed independently by various laboratories. The only thing that is shared at the beginning of such independent investigations is the agreed periodic micro-geometry of the porous materials developed in that way.

The influence of additive manufacturing processes on the sound absorption of a few materials with designed porosity has already been reported [26, 27]. The current paper presents most of the results obtained from the measurements of over 90 samples manufactured in 7 different AM technologies on 16 AM devices (15 different) in six laboratories and acoustically tested by the sample manufacturers and also in three other laboratories to ensure the correctness of the measurements. For most samples of the same periodic micro-geometry, good and sometimes very good consistency of the measurement results was obtained, which together with their microscopic examination allows to indicate technologies, materials and devices capable of the best reproduction of the designed microstructure. It seems that such comparative acoustic tests can also be used to assess the quality of reproduction of designed materials with fine details. The outline of this paper is as follows. The periodic geometries of the porous samples are described in Section 2. Then, the manufacturing techniques are briefly discussed and samples produced using them are presented in Section 3. The whole scheme of the round robin study including sample production and acoustic tests in the impedance tube using the transfer function method with two microphones [28–30] is discussed in Section 4. Finally, the measurement results are compared in Section 5.

2. Periodic porosity designs

2.1. One-Pore-Cell geometry

Two kinds of cubic cells with periodic porosity were designed for this study. In both cases, the periodic porosities are completely open and consist of spherical pores connected by short cylindrical channels.

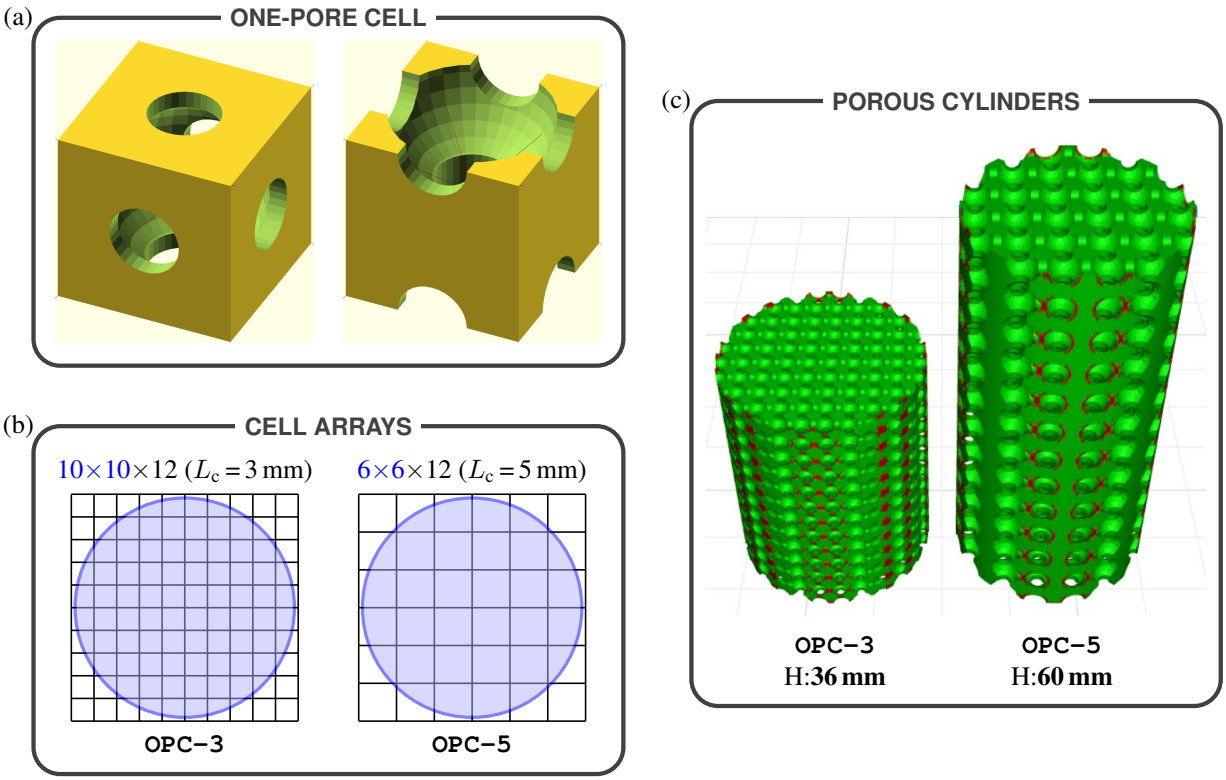

Figure 1: One-Pore Cell (OPC) geometry: (a) two alternative representations of the periodic cell, (b) arrays of cells (L_c = 3 mm or 5 mm) for CAD models of samples with a diameter of 29 mm, (c) CAD models of the periodic cylindrical samples OPC-3 and OPC-5 (diameter about 29 mm and height 36 mm or 60 mm, respectively)

The first periodic cell is very simple: it contains a single spherical pore that is connected to identical pores of neighbouring cells through very short (horizontal or vertical) channels of the same size. The pore diameter is $0.9L_c$ and the channel diameter is $0.4L_c$, where L_c is the size (length of the edge) of the cubic cell. This One-Pore Cell (OPC) is depicted in Figure 1(a) in two alternative representations: with the pore in the centre of the cube and with the pore shifted vertically from this position by half the size of the cube. The latter version was used to generate two types of CAD geometry for porous cylindrical samples shown in Figure 1(c). For the first CAD geometry of the cylindrical sample, the cubic cell size was set to $L_c = 3$ mm, and then a three-dimensional array of $10 \times 10 \times 12$ cells was constructed, see Figure 1(b), from which a vertical cylinder with a diameter of 29 mm and a height of 36 mm was cut. Cylindrical samples with this periodic microstructure will be designated as OPC-3 samples. For the second CAD geometry the cubic cell size was set to $L_c = 5$ mm and a vertical cylinder with a diameter of 29 mm was cut from the array of $6 \times 6 \times 12$ such cells so that its height is 60 mm, see Figure 1(b,c). These higher cylindrical samples with larger pores will be designated as OPC-5 samples.

CAD geometry models for OPC-3 and OPC-5 samples with larger diameters are constructed in a similar way only the cell array must be larger in both horizontal directions, for example, for a diameter of 40 mm the cell array must have $14 \times 14 \times 12$ cells for OPC-3, and (at least) $8 \times 8 \times 12$ cells for OPC-5. If a sample is to be 3D printed with a diameter slightly larger than 40 mm (for example, to cut it to fit later), then the number of cells in both horizontal directions must be even larger but always even (not odd). Although the CAD geometry for OPC samples can be easily built with any CAD tool, we provide *OpenSCAD* code for OPC samples in Table A.1 in the Appendix. This code automatically adheres to the above rules when the user sets only the cell size and sample diameter.

2.2. *Four-Pore-Cell geometry*

The second periodic cell with open porosity is more complex than the previous one because it was built randomly. A periodic arrangement of four spherical pores of different sizes in a cubic cell was randomly generated using the algorithm proposed in [31]. The central point of the cubic cell was moved to the centre of the smallest pore, and the whole system was scaled (normalised), so that the size (edge) of the cubic cell is 1. Then, the normalised positions (centres) and pore diameters were rounded to two decimal places. The normalised values of pore diameters, i.e. 0.59, 0.64, 0.67, and 0.76, respectively, will be reduced by 10% as explained below. Because the pore diameter is smaller than the size of a cubic cell, only one instance of central pore is in the cubic cell. On the other hand, for each of the other three pores, four periodically shifted pore instances are partly in the same cubic cell, which means that together there are 13 instances of 4 different pores in such a Fore-Pore Cell (FPC). This initial FPC design is shown in the top frame in Figure 2 for three different orientations of the periodic cell. The bottom row in this frame shows the results of analyses carried out by the *Z-suite* slicing software (dedicated for *Zortrax* 3D printers) for the periodic cell scaled to the size of 5 mm. These analyses show that the wide fragments of the edges around the windows connecting the pores are too thin to be properly 3D printed using *Zortrax M200* 3D printer (or other FDM devices with a standard nozzle size of 0.4 mm), and un-designed windows (holes) will also be created, because some parts of the wall between the pores are too thin. Therefore, the diameters of all the pores were reduced by 10% and rounded again to two decimal places (see the middle frame in Figure 2), and then cylindrical channels were set between each pair of pores that were originally connected by windows. To accurately re-create these connections, the normalised diameters of the cylindrical channels were set to the values found for the windows in the initial design (rounded to two significant digits). In this way, the edges of the windows are now thick enough so that they can be manufactured correctly using FDM devices (see the final design in the bottom frame in Figure 2). This and other crucial issues relevant to the FDM technology are studied, e.g., in [32].

All the necessary data for the final FPC design is given in Table 1 for the cell orientation designated FPC-Z, because the axis of the porous cylinder of the corresponding FPC-Z sample is along the Z-axis. Two other orientations will also be used, namely: FPC-X when the axis of the porous cylinder of the respective sample is along the X-axis, and FPC-Y when it is along the Y-axis. The porous cylinders are

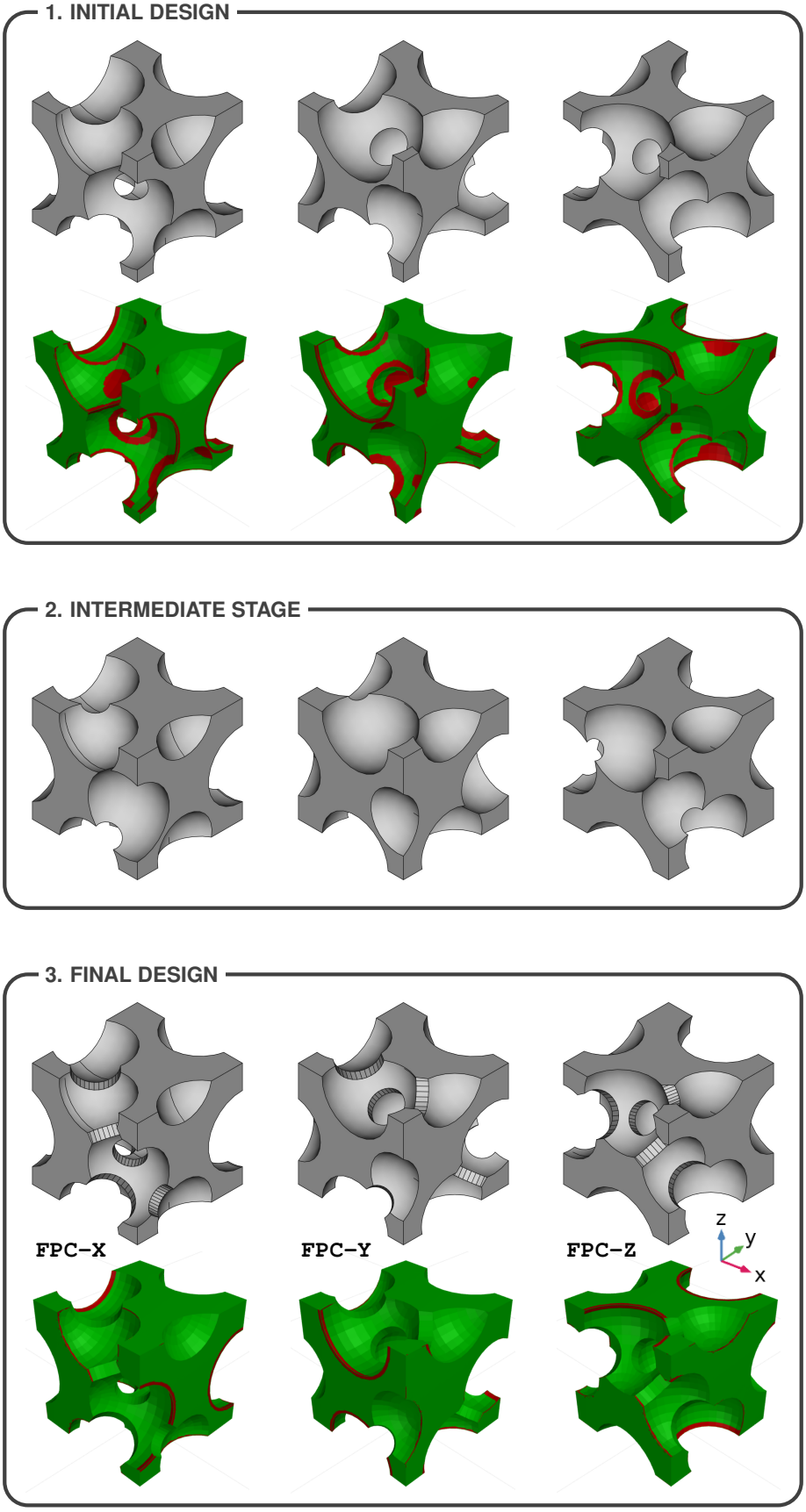

Figure 2: Four-Pore Cell (FPC) geometry: a re-design procedure and three orientations

upright, so in practice the FPC cell is rotated, and therefore the FPC-X cell is obtained by rotating FPC-Z cell by 90° around the Y-axis, while the FPC-Y one by rotating the FPC-Z cell by 90° around the X-axis. The normalised values are given in Table 1 and they must be scaled by $L_\mathrm{c} = 5\,\mathrm{mm}$, which is the size

Table 1: Data for FPC geometry with the cubic cell centred on `[0,0,0]` and edge length `1`

Diameters of pores and positions all relevant pore instances

No.	Pore instance	Pore diameter	Coordinates of the pore centre $[x, y, z]$		
1	P1-1	0.53	0.00	0.00	0.00
2	P2-1	0.58	-0.47	-0.44	0.04
3	P2-2	0.58	0.53	-0.44	0.04
4	P2-3	0.58	-0.47	0.56	0.04
5	P2-4	0.58	0.53	0.56	0.04
6	P3-1	0.60	0.45	-0.05	-0.35
7	P3-2	0.60	-0.55	-0.05	-0.35
8	P3-3	0.60	0.45	-0.05	0.65
9	P3-4	0.60	-0.55	-0.05	0.65
10	P4-1	0.68	0.04	-0.51	0.37
11	P4-2	0.68	0.04	0.49	0.37
12	P4-3	0.68	0.04	-0.51	-0.63
13	P4-4	0.68	0.04	0.49	-0.63

Diameters of channels between relevant pore instances

Pore instance	Pore instance	Channel diameter
1 (P1-1)	6 (P3-1)	0.26
1 (P1-1)	10 (P4-1)	0.24
1 (P1-1)	11 (P4-2)	0.27
2 (P2-1)	7 (P3-2)	0.34
2 (P2-1)	10 (P4-1)	0.34
3 (P2-2)	6 (P3-1)	0.34
3 (P2-2)	10 (P4-1)	0.37
4 (P2-3)	11 (P4-2)	0.34
5 (P2-4)	11 (P4-2)	0.37
6 (P3-1)	12 (P4-3)	0.23
8 (P3-3)	10 (P4-1)	0.23

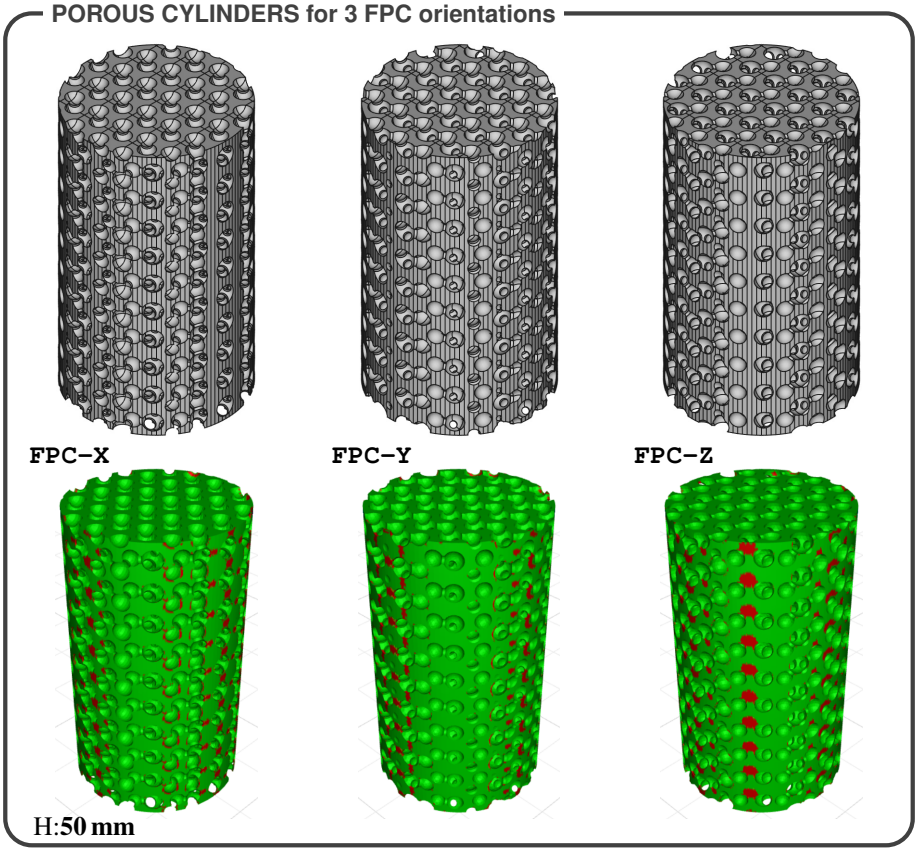

Figure 3: CAD models for FPC samples (diameter about 29 mm and height 50 mm) – generated in *FreeCAD* (upper row) and analysed in *Z-Suite* (lower row)

(length of the edge) of the cubic cell. CAD models for FPC samples are obtained in a similar way as for OPC-5 samples, cf. Figure 1(b), but the cylinder height is 50 mm (not 60 mm), so for example, the CAD models for samples with a diameter of 29 mm shown in Figure 3 were cut from three-dimensional arrays with $6 \times 6 \times 10$ (not 12) cells. We provide *OpenSCAD* code for FPC samples in Tables A.2 and A.3 in the Appendix. The cell size for FPC samples is fixed to 5 mm, so the user sets only the cell orientation and sample diameter.

3. Manufacturing of samples

3.1. Additive Manufacturing technologies and devices

Periodic porous samples with microstructure designs proposed in Section 2 were fabricated in seven AM technologies that are briefly presented below [6, 7, 9, 11, 33, 34]. The brand names of 15 different 3D printing devices used in this study are also provided.

FDM: Fused Deposition Modelling, a.k.a. Fused Filament Fabrication (**FFF**) or Layer Plastic Deposition (**LPD**), is probably the cheapest, easiest in service, and the most common method. In it a solid polymer is heated up in the extruder to the melting temperature and injected through a nozzle onto a platform, where it solidifies again when cooled. Once the cross-section pattern of a given layer is formed, the nozzle moves up by a certain distance (called the layer thickness) and starts to build the next layer by pushing a specific amount of the thermoplastic material to particular places. The process continues until the whole object is completed. If it contains overhanging features, the application of additional supports may be inevitable. FDM 3D printers used in this study: *Zortrax M200*, *Flashforge Creator Pro*, *Makerbot Replicator Z18*, *Creality Ender 3*, *Ultimaker 2*.

DMLS: In Direct Metal Laser Sintering, small particles of metal are joined together by a high-power laser. During the production cycle, the working platform is repeatedly lowered by a single layer thickness, and the fresh powder is tipped into it from the source bed by the recoater. Then, the laser follows a predefined path such that the shape of the current layer is finally reflected. In contrast to the FDM technology, support material is not needed as this purpose is served by an unsintered material. DMLS 3D printer used in this study: *EOS EOSINT M280*, *Sisma MYSINT100*.

SLM: Selective Laser Melting technique has many in common with DMLS. The distinction between the two is often far from clear and relates mostly to patent restrictions as well as innovative solutions implemented like the recoater material – rubber in SLM and steel or ceramic in DMLS. SLM 3D printer used in this study: *3D Systems ProX*.

SLS: Selective Laser Sintering is very similar to DMLS or SLM in operation. The main difference is in the applied laser and material. SLS is intended to work with polymer (e.g. nylon PA12, etc.) powders of grain size about 30 to 40 micrometres. SLS 3D printers used in this study: *Sinterit Lisa*, *3D Systems ProJet 160*.

SLA: Stereolithography is based on exposing to light a liquid photopolymer resin and causing it to cure in a layer-by-layer fashion. In this technology the curing process is done by a laser beam directed by galvanometers onto particular points on a build platform or an object partially immersed in the pool of resin. In principle, SLA requires dedicated supports to yield best quality parts. However, the porous samples of the proposed micro-geometry were printed without them, because they were not necessary. SLA 3D printers used in this study: two devices *Formlabs Form 2*.

DLP: In Digital Light Processing, like in SLA technology, the liquid photopolymer is solidified by light, although coming from different source. As opposed to SLA, in DLP technology the light is emitted from a projector and guided to the predefined points by a sequence of mirrors (a Digital Mirror Device). DLP 3D printers used in this study: *Kudo3D Titan 1*, *Autodesk Ember*.

LCD: In this technology, sometimes called LCD-based SLA or UV LCD, the liquid photopolymer is also cured by light. However, despite generally the same principle of operation, LCD 3D printers do not have any laser in them but cure the entire layer of photopolymer resin at once using a liquid-crystal display (LCD) screen with ultraviolet light-emitting diode backlighting. This approach is much faster than SLA, and independent of the dimensions of fabricated objects. LCD 3D printers used in this study: *Zortrax Inkspire*, *Anycubic Photon*.

The overall quality of some of the obtained porous samples was assessed on a series of measurements of crucial dimensions made with the aid of digital microscopes. It was observed that the designed microstructure was precisely reflected only for the case of the resin samples (SLA and LCD). Other technologies provided rough surfaces, indistinct edges, more or less degenerated pores (especially near the cylindrical surface of a sample), and were not able to capture important albeit intricate details. Furthermore, the spherical voids present in the microstructure turned out to have smaller diameters than anticipated and were distributed by unintended distances. The reason for this is twofold: the highest printing resolution offered by SLA, LCD, and also DLP (with the lower limit of 25 microns) and the usage of a liquid material. Nevertheless, resin samples must be carefully post-processed (cleaned and exposed to light for some time after fabrication to enhance solidification) in order to avoid shrinkage over time. Because the LCD screen is composed of a number of pixels, the layers generated in the LCD technique consist of so-called voxels, a spatial equivalent of pixels. This is why LCD prints are usually slightly more rough than the SLA ones, but still their quality is better when compared to samples fabricated in a low-resolution technique of FDM, or even in finer SLS and DLMS or SLM techniques. It should be also noted that obtaining FDM samples with small details of decent quality usually require some experience in the selection of materials and 3D printing parameters.

3.2. Samples manufactured for impedance tubes with a diameter of 29 mm

Periodic porous samples dedicated for 29 mm impedance tubes were manufactured by: (1) IPPT using FDM (*Zortrax M200* and *Flashforge Creator PRO*), SLS (*Sinterit Lisa*), DMLS (*EOSINT 280*), and LCD (*Zortrax Inkspire*) technologies, (2) UTC using FDM (*Makerbot Replicator Z18*), SLS (*3D Systems ProJet 160*), and SLA (*Formlabs Form 2*) technologies, and (3) EMPA using *Kudo3D Titan 1* in DLP technology and *Sisma MYSINT100* in DMLS technology.

Complete sets of OPC and FPC samples were manufactured by IPPT in four completely different technologies. Figure 4 shows some of these samples. It should be noted that two different FDM devices (*Zortrax M200* and *Flashforge Creator PRO*) were used to produce several sets of samples in this

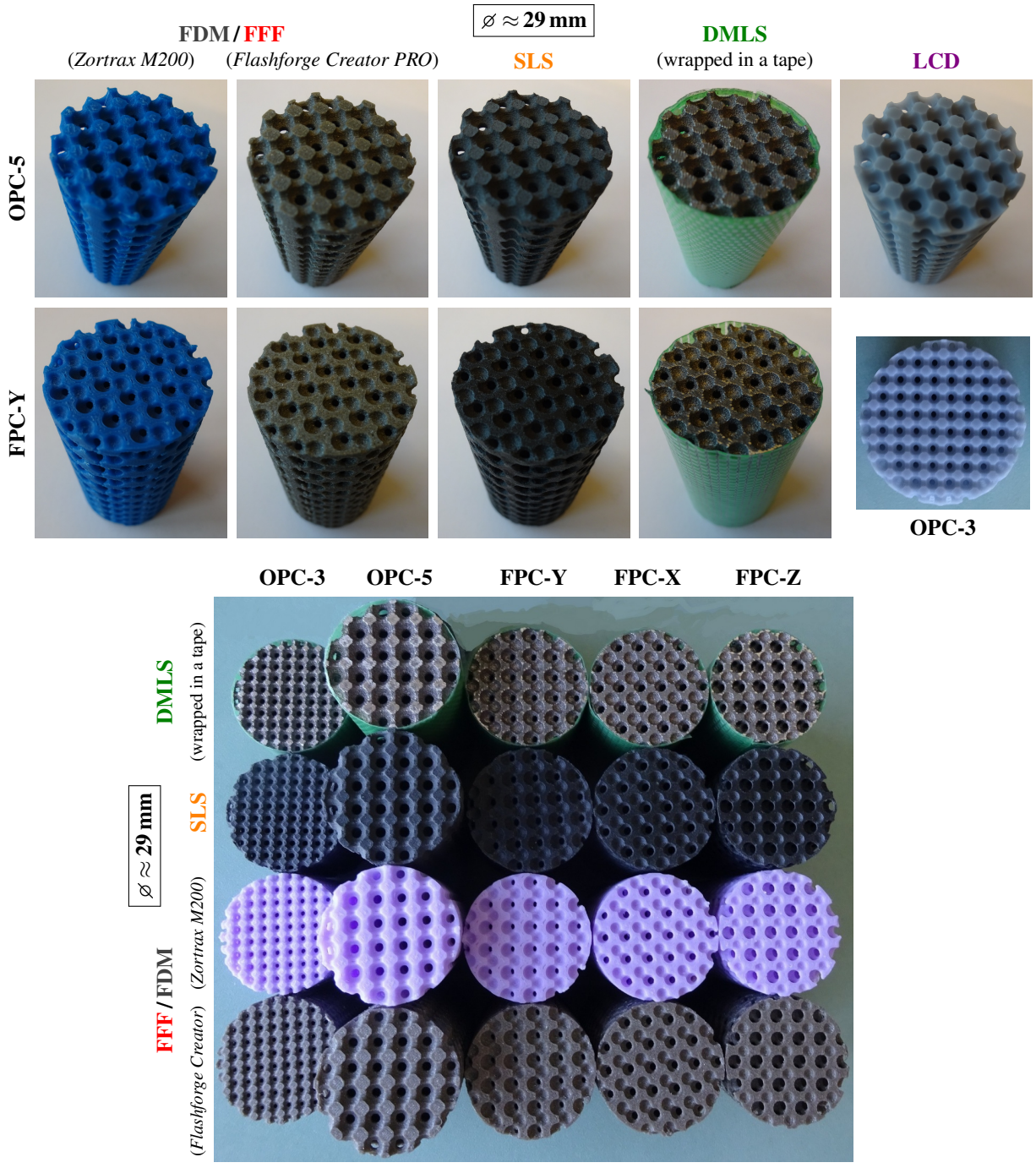

Figure 4: Some of the OPC and FPC samples ($\varnothing \approx 29$ mm) manufactured by IPPT using FDM/FFF, SLS, DMLS, and LCD technologies

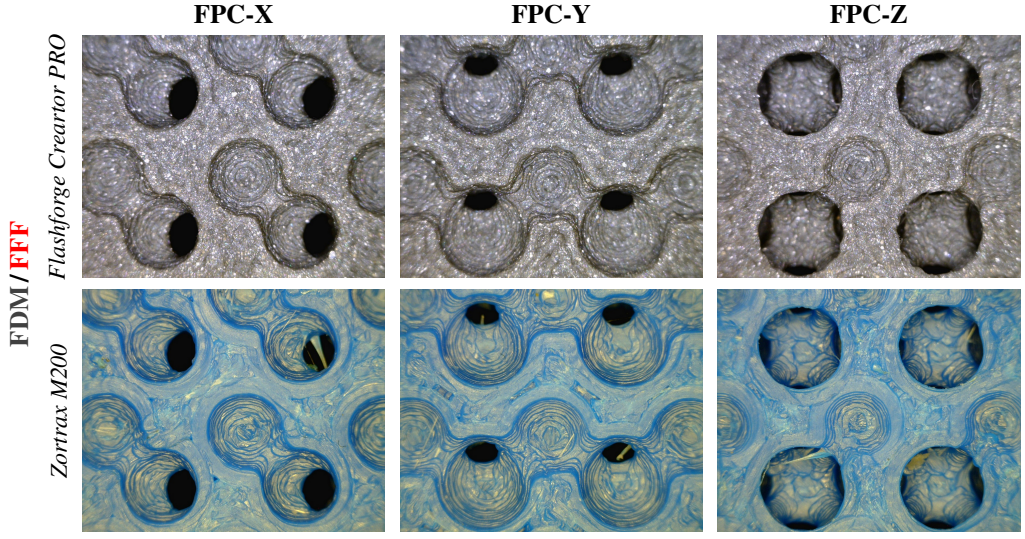

Figure 5: Zoomed surfaces of FPC samples manufactured by IPPT using two different devices in FDM/FFF technology

technology which allowed to observe that the quality and surface features of the samples obtained from the same AM device and material were virtually the same. On the other hand, one can easily notice differences between samples produced using different AM technologies and even different devices of the same technology FDM. This is well illustrated in Figure 5 where surfaces for the FPC samples manufactured using *Flashforge Creator PRO* are compared with the ones from *Zortrax M200*. A relatively high quality of samples produced with *Flashforge Creator PRO* was obtained after many tests involving experimenting with 3D-printing parameters and various high quality ABS (acrylonitrile butadiene styrene) materials from different producers (the final choice was *Rigid.Ink*), whereas a good quality from *Zortrax M200* was achieved using a dedicated high quality ABS material *Z-Ultrat* and parameters set up for this material by the 3D-printer producer. The diameter of metal samples produced in DMLS technology was deliberately chosen so that these samples loosely fit the 29 mm impedance tube and they must be

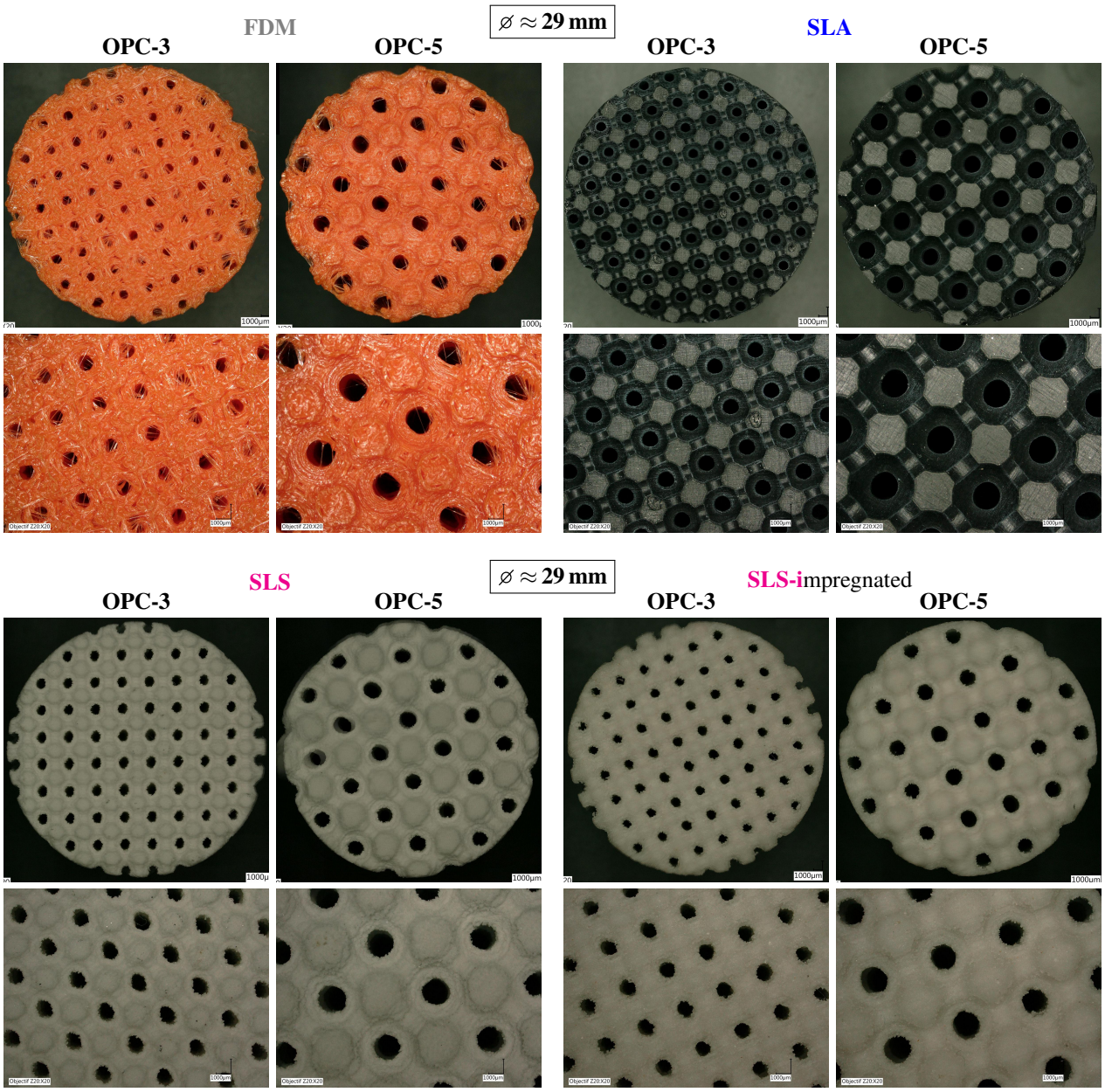

Figure 6: OPC samples ($\varnothing \approx 29$ mm) manufactured by UTC using FDM, SLA, and SLS technologies

wrapped in a tape for a tight fit (see the green tape around these samples in Figure 4). This had to be done (even knowing that the presence of the tape would affect the measurements) to avoid scratching the inside of the tube. The SLS samples were printed on *Sinterit Lisa* with a layer thickness equal 0.075 mm (the thinnest possible layer).

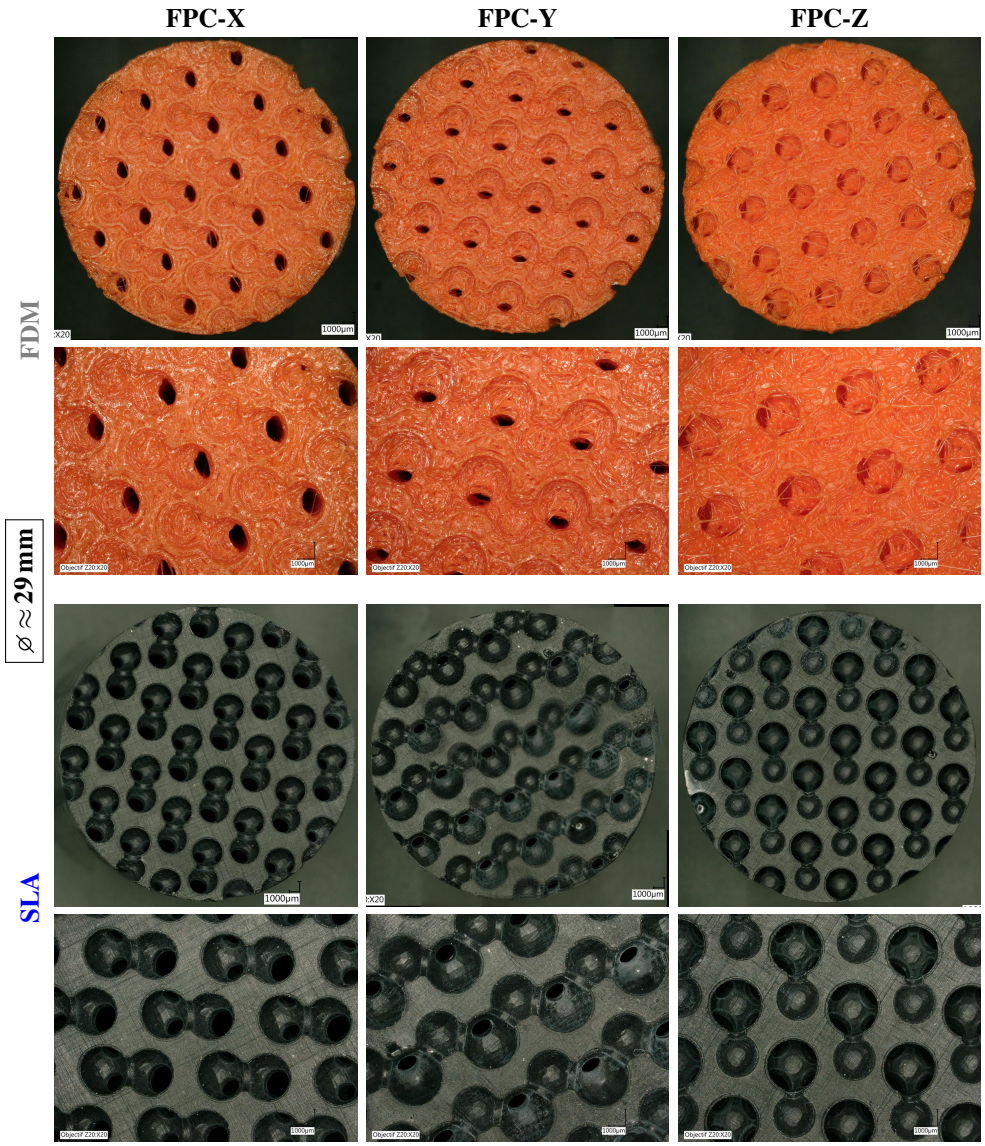

Figure 7: FPC samples ($\varnothing \approx 29$ mm) manufactured by UTC using FDM and SLA technologies

Figures 6–8 present the samples manufactured by UTC. This laboratory used three different AM technologies to produce complete sets of OPC (see Figure 6) and FPC samples (see Figures 7 and 8), however, in the case of SLS technology the samples were impregnated with cyanoacrylate to close the micro-pores that were present because of the relatively large grains of the polymer powder used in the sintering process, so that pictures of the SLS samples before and after impregnation are shown in Figures 6 and 8. Microscopic examinations of the samples (see enlarged photographs of their surfaces in Figures 6–8) allowed to assess the relative quality of workmanship using different technologies. In the case of FDM sample quality is generally poor (when compared to the FDM samples produced by IPPT): the channels and pores are distorted and the surface is rough with tiny polymer fibres which often run

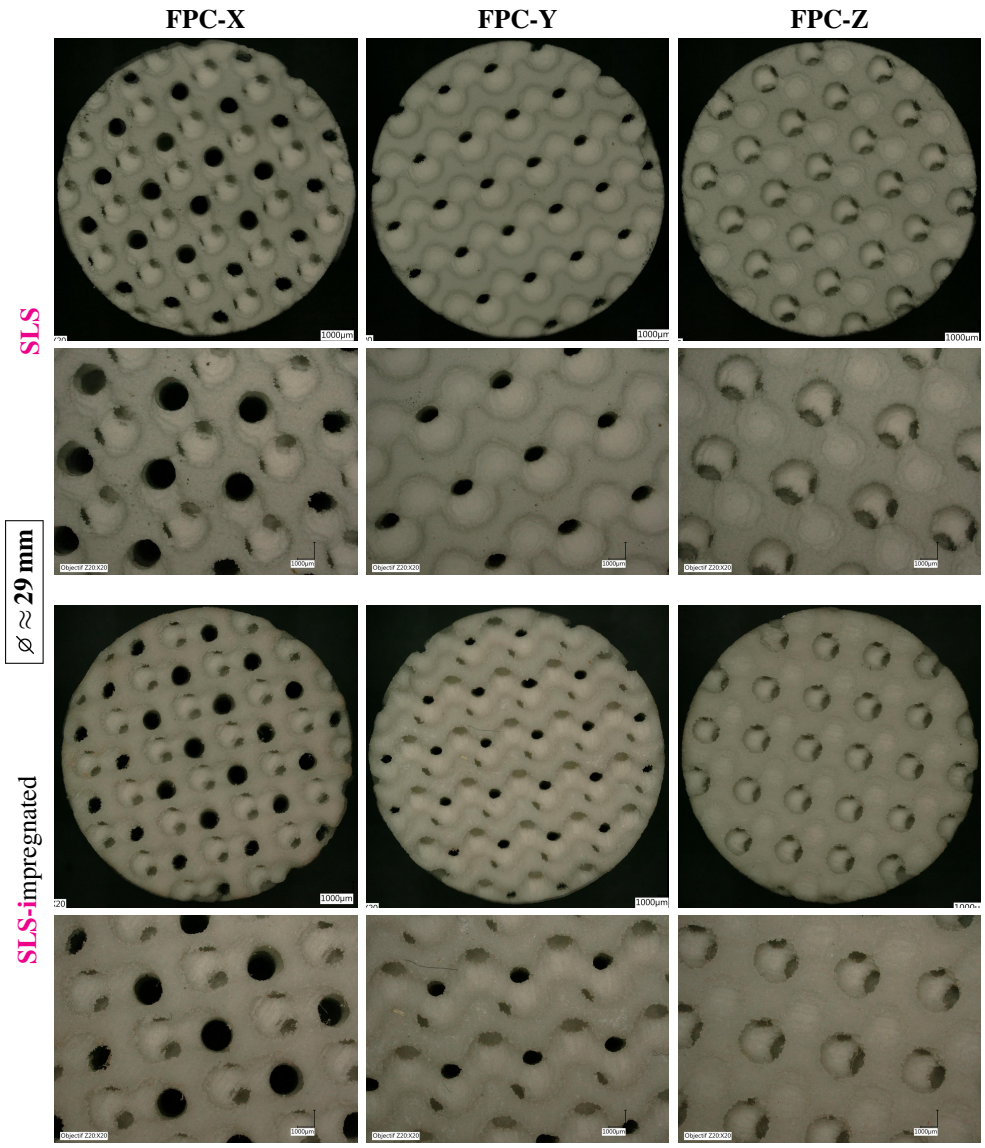

Figure 8: FPC samples ($\varnothing \approx 29$ mm) manufactured by UTC using SLS technology

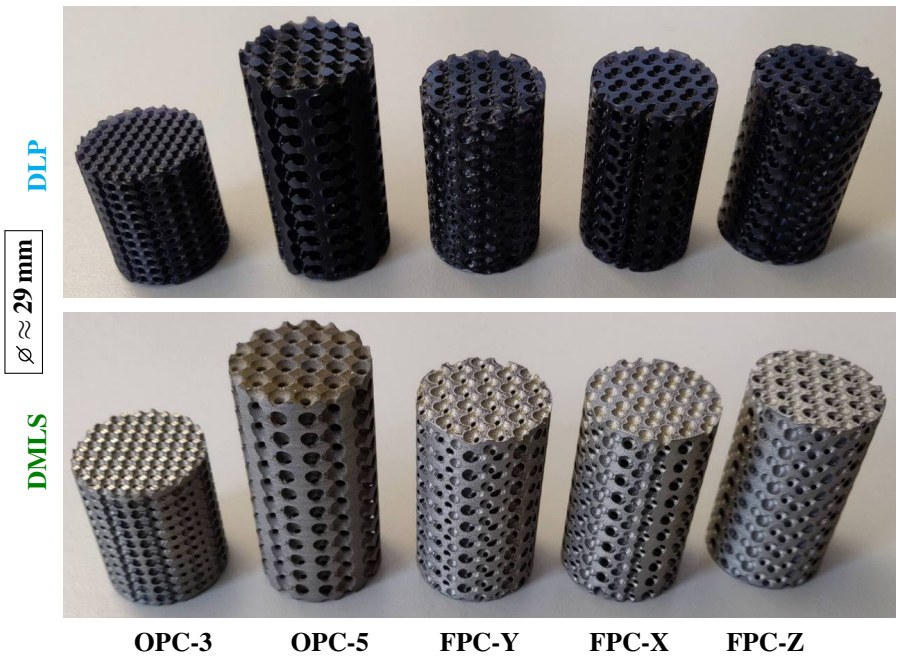

Figure 9: OPC and FPC samples ($\varnothing \approx 29$ mm) manufactured by EMPA using DLP and DMLS technologies

across the channels and pores. On the other hand, the shape and surface quality of SLA samples produced by UTC from photopolymer resin is excellent when compared with other technologies: the surfaces are very smooth and the shapes of circular channels and spherical pores are not distorted.

EMPA produced complete sets of high-quality OPC and FPC samples from photopolymer resin using DLP technology and metal samples from stainless steel powder in DMLS technology (see Figure 9). The metal samples were wrapped with tape to fit it securely into the impedance tube.

3.3. Samples manufactured for impedance tubes with diameters of 40 mm and 30 mm

Periodic porous samples for testing in 40 mm impedance tubes were manufactured by: (1) TCD using FDM (*Creality Ender 3*), SLM (*3D Systems ProX*), SLA (*Formlabs Form 2*), and DLP (*Anycubic Photon*) technologies, (2) TUe using *Ultimaker 2* in FDM technology, and (3) IPPT using *Zortrax M200* in FDM technology and *Sinterit Lisa* in SLS technology.

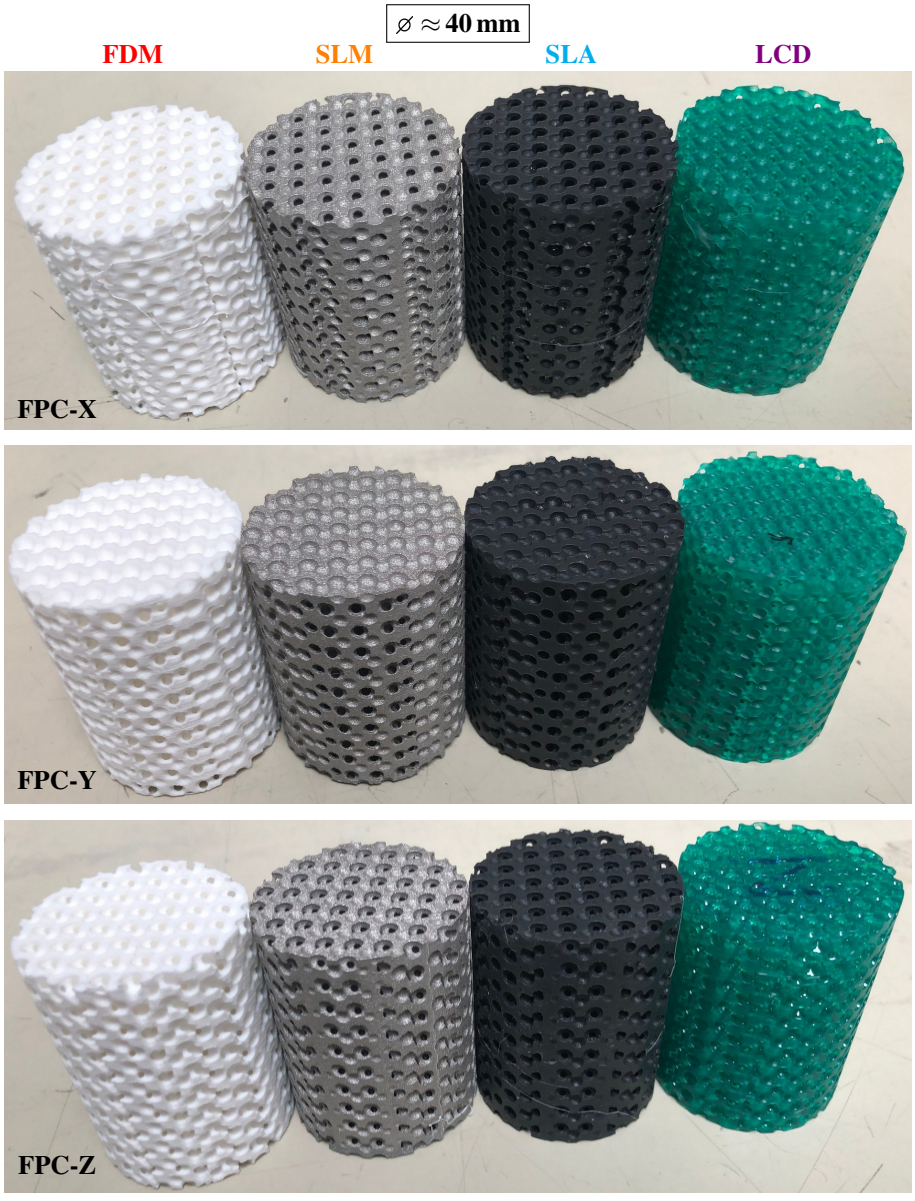

Figure 10: FPC samples (⌀ ≈ 40 mm) manufactured by TCD using FDM, SLM, SLA, and LCD technologies

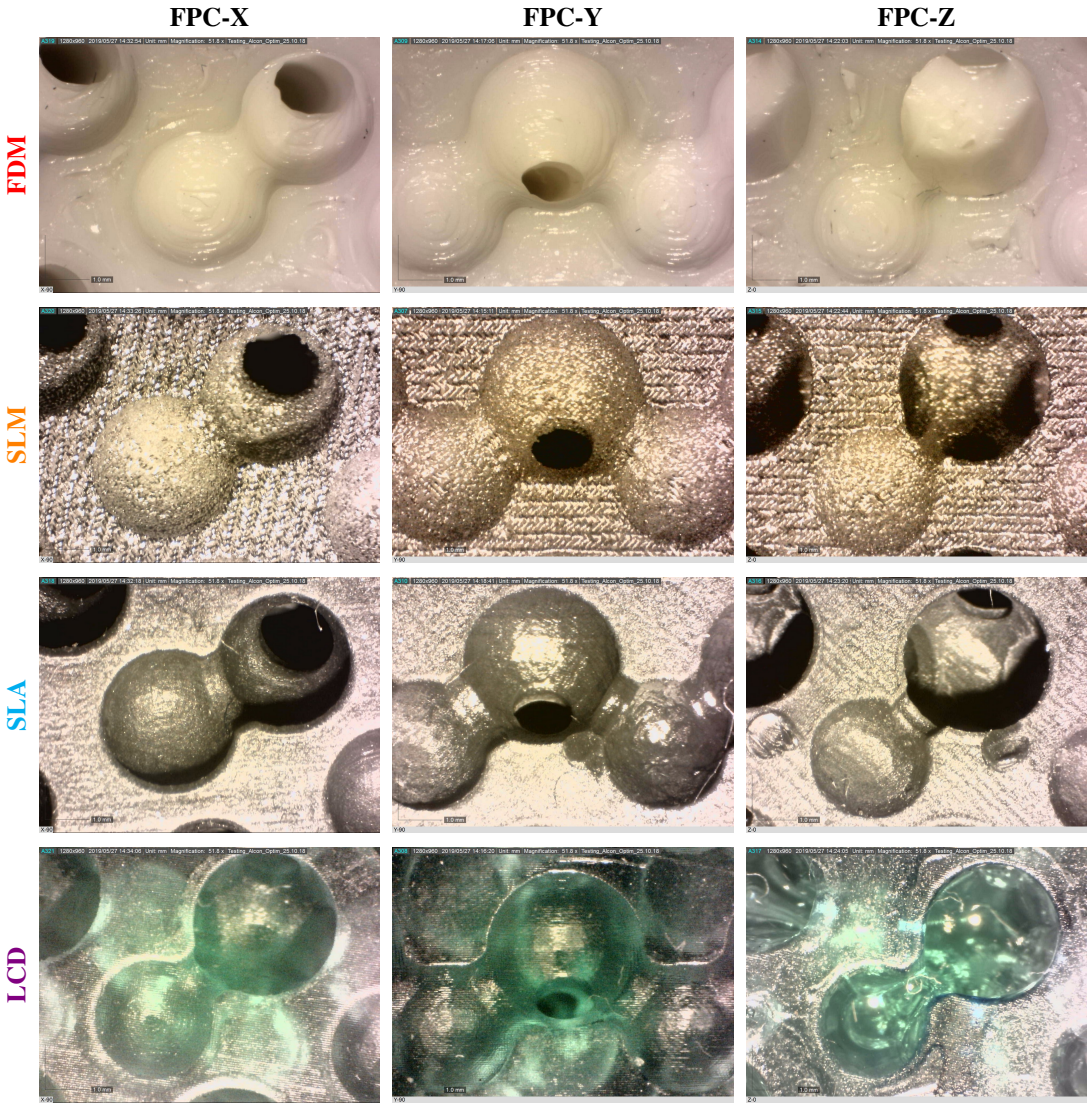

Figure 11: Zoomed surfaces of FPC samples manufactured by TCD

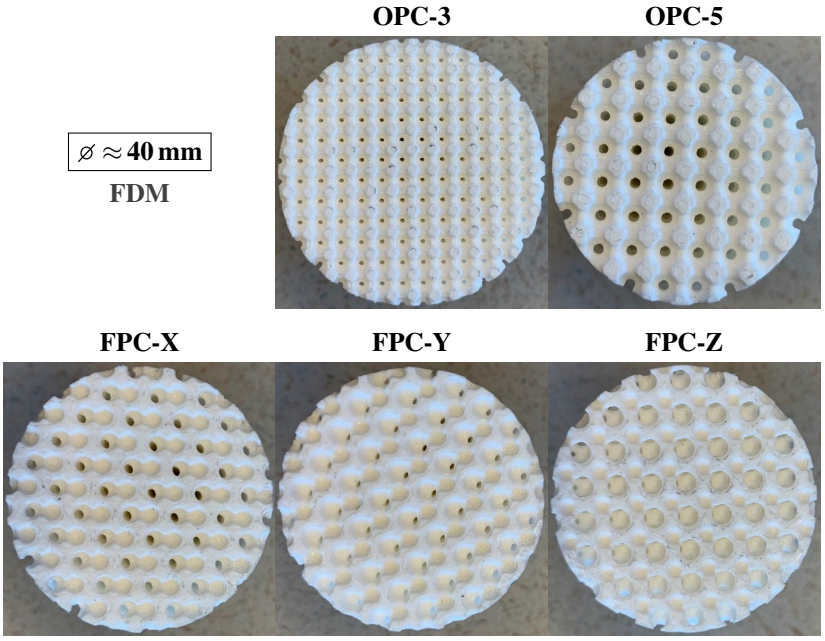

Figure 12: OPC and FPC samples ($\varnothing \approx 40$ mm) manufactured by TUe in FDM technology

Figure 10 presents the FPC samples produced by TCD from ABS polymer filament, metal powder, and photopolymer resins. The metal samples were manufactured from cobalt-chromium powder in SLM technology and they were wrapped with tape before being inserted into the impedance tube for acoustic testing. The pictures of top surfaces of these samples taken under a microscope are shown in Figure 11. When comparing the resin samples it was observed that the quality of the ones manufactured in LCD technology was inferior than that of the samples in SLA technology. This is mainly because some channels in LCD samples were clogged by the resin (in particular, in the case of FPC-X sample) that was not completely removed.

The top surfaces of OPC and FPC samples produced by TUe in FDM technology are shown Figure 12. The quality of these samples is average: their surface is moderately uneven, but without fibres,

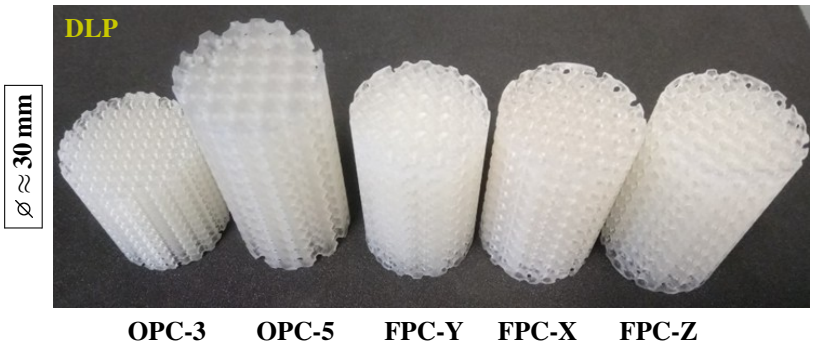

Figure 13: OPC and FPC samples ($\varnothing \approx 30$ mm) manufactured by MIT in DLP technology

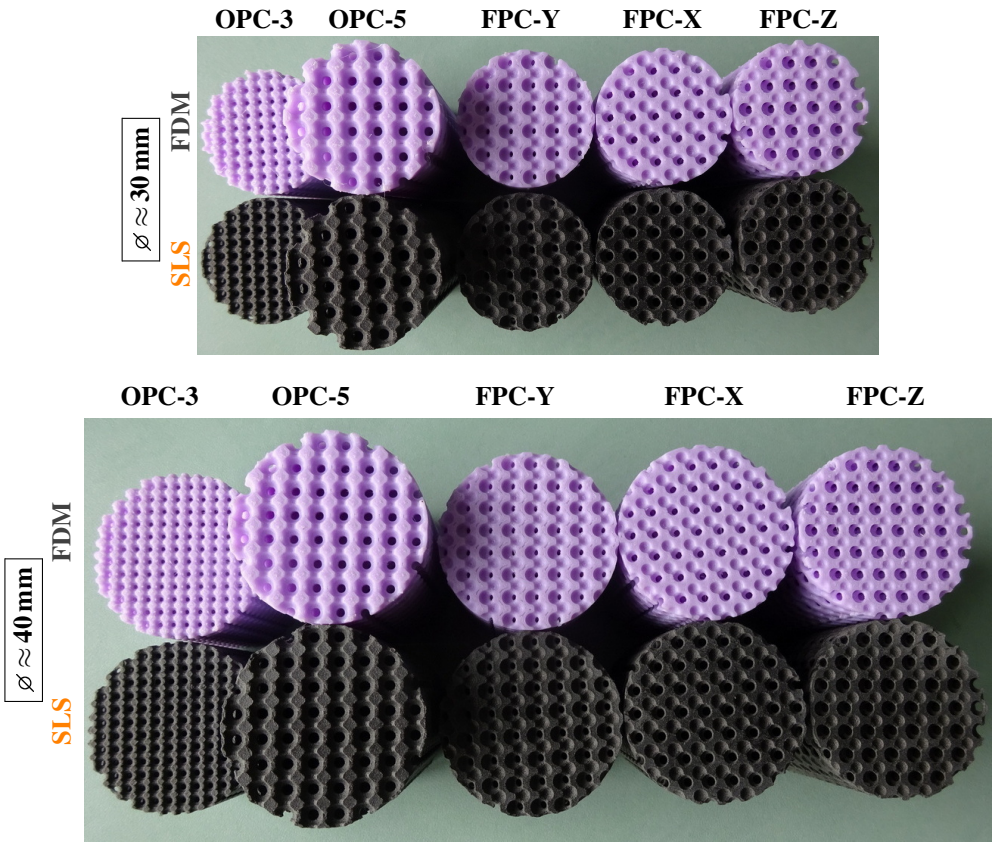

Figure 14: OPC and FPC samples ($\varnothing \approx 30$ mm and $\varnothing \approx 40$ mm) manufactured by IPPT using FDM and SLS technologies

however the shape mapping is rather rough. Their overall quality is estimated to be lower than the samples manufactured with *Flashforge Creator PRO* or *Zortrax M200*, comparable to the samples manufactured with *Creality Ender 3*, and higher than the samples manufactured with *Makerbot Replicator Z18*.

Periodic porous samples for testing in 30 mm impedance tubes were manufactured by: (1) MIT using *Autodesk Ember* in DLP technology, and (2) IPPT using *Zortrax M200* in FDM technology and *Sinterit Lisa* in SLS technology.

The OPC and FPC samples manufactured by MIT in DLP technology are shown in Figure 13. Their quality was good, comparable with the high quality of resin samples manufactured in SLA technology by UTC, EMPA, and TCD. Figure 14 presents the complete sets of OPC and FPC samples manufactured by IPPT in FDM and SLS technologies, dedicated for testing in other laboratories having impedance tubes with an inner diameter of 30 mm (LAUM) or 40 mm (KUL).

4. Round robin investigations

Table 2 lists the nine laboratories involved in the round robin studies on sound-absorbing media with periodic open porosity produced using various Additive Manufacturing technologies. Six of these laboratories manufactured a different number of samples with diameters suitable for the impedance tubes used by them to measure acoustical properties of materials, viz.: 29 mm (IPPT, UTC, EMPA), 30 mm (MIT), and 40 mm (TCD, TUe). In addition, IPPT manufactured also sets of samples for tubes with diameters of 30 mm and 40 mm.

Seven different AM technologies (FDM, SLS, DMLS, SLM, SLA, DLP, LCD) were used to produce the samples from four kinds of input materials, namely: ABS polymer filaments, polymer powders, metal powders (aluminium, stainless steel, or cobalt-chrome), and photopolymer resins. The types of samples produced by each of the six laboratories are listed in Table 2 together with the appropriate AM technology and 3D-printing device. Although the samples were acoustically tested by their manufacturers, in addition their acoustic properties were also measured in other laboratories, namely: the 29 mm samples produced by IPPT and UTC were independently tested by ECL, the 30 mm samples produced by MIT and IPPT were tested by LAUM, and finally, the 40 mm samples (delivered by TUe and IPPT) were tested by KUL. It should be noted that although IPPT produced samples for all considered impedance tube diameters (i.e. 29 mm, 30 mm, and 40 mm), it tested only those that fit in a 29 mm tube.

During the round robin investigations more than 90 samples were acoustically tested in impedance tubes, the majority of them in (at least) two different laboratories. The complete test for one sample consisted in measurements of the surface acoustic impedance and acoustic absorption for the sample in three (or, in fact six) configurations. First, the sample was placed with its bottom face directly on the rigid termination of the impedance tube so that its upper face was impinged by acoustic plane waves at normal incidence. Then, an air gap of 20 mm was created between the sample and the rigid termination by moving the rigid plunger, and the measurement was repeated. A final measurement was taken for

Table 2: Laboratories involved in round robin manufacturing and testing of periodic porous samples, the corresponding impedance tube sizes, AM technologies and devices, types of materials, and manufactured samples (OPC = 2 samples: OPC-3 and OPC-5; FPC = 3 samples: FPC-X, FPC-Y, and FPC-Z)

Institution (laboratory)	**Tube size** ≈ sample ⌀	**FDM/FFF** ABS polymer	**SLS** polyamid powder	**DMLS SLM** metal powders	**SLA DLP LCD** photopolymer resins
IPPT	**⌀ 29 mm**	OPC [(1)], FPC [(1)] *Zortax M200* *Flashforge Creator PRO*	OPC, FPC *Sinterit Lisa*	OPC, FPC *EOSINT M280*	OPC *Zortrax Inkspire*
	⌀ 30 mm[(2)]	OPC, FPC *Zortax M200*	OPC, FPC *Sinterit Lisa*		
	⌀ 40 mm[(2)]	OPC, FPC *Zortax M200*	OPC, FPC *Sinterit Lisa*		
UTC	**⌀ 29 mm**	OPC, FPC *Makerbot Replicator Z18*	OPC [(3)], FPC [(3)] *3D Systems ProJet 160*		OPC, FPC *Formlabs Form 2*
EMPA	**⌀ 29 mm**			OPC, FPC *MYSINT100*	OPC, FPC *Kudo3D Titan 1*
MIT	**⌀ 30 mm**				OPC, FPC *Autodesk Ember*
TCD	**⌀ 40 mm**	FPC *Creality Ender 3*		FPC *3D Systems ProX*	FPC *Formlabs Form 2* FPC *Anycubic Photon*
TUe	**⌀ 40 mm**	OPC, FPC *Ultimaker 2*			

[(1)] A few complete sets of these samples were manufactured using two different FDM/FFF devices.
[(2)] IPPT only manufactured samples of this diameter (i.e. acoustic tests were carried out by another laboratory).
[(3)] These samples were acoustically tested and then impregnated with cyanoacrylate and tested again.

ECL	**⌀ 29 mm**	acoustical testing of samples from UTC and 29 mm samples from IPPT
LAUM	**⌀ 30 mm**	acoustical testing of samples from MIT and 30 mm samples from IPPT
KUL	**⌀ 40 mm**	acoustical testing of samples from TUe and 40 mm samples from IPPT

IPPT : Institute of Fundamental Technological Research of the Polish Academy of Sciences (Poland)
UTC : Université de Technologie de Compiègne (France)
EMPA : Swiss Federal Laboratories for Materials Science and Technology (Switzerland)
MIT : Massachusetts Institute of Technology (USA)
TCD : Trinity College Dublin (Ireland)
TUe : Eindhoven University of Technology (the Netherlands)
ECL : Ecole Centrale de Lyon (France)
LAUM : Laboratoire d'Acoustique de l'Université du Mans (France)
KUL : KU Leuven (Belgium)

the case when the air gap was increased to 40 mm. This three-measurement procedure was repeated for the inverted sample so that its bottom face was exposed to incident plane acoustic waves. Inverted sample measurements generally confirmed the previous results very well, although especially in the case of FDM technology and metal samples, the bottom surface of a sample (which is in one way or another connected to the platform during the 3D printing process) usually slightly differs from the upper one. It was observed, however, that this effect was rather negligible since all discrepancies between two measurements – in the standard and inverted position, respectively – were not significant and occurred at higher frequencies (above 5 kHz) where the other factors (i.e. material, manufacturing technology, etc.) are much more important and usually cause more discrepancies.

The round robin tests allowed to create a database of acoustical measurements obtained for samples manufactured in different AM technologies and measured by independent laboratories. The results were analysed and compared, in particular, for the samples with the same periodic microstructure. Most

Table 3: Result labels used in Figures 15–24, combined with the corresponding impedance tube diameters used for measurements, additive manufacturing devices and materials, and involved laboratories

Result label	**Tube size** ≈ sample ⌀	***3D-printing device* [& material]**	**Manufactured & tested by**	**Independent testing by**
FDM-IPPT	⌀ **29 mm**	*Zortrax M200* [polymer filament ABS (Z-Ultrat)]	IPPT	ECL
FFF-IPPT **FFF**-IPPT*		*Flashforge Creator PRO* [polymer filament ABS]	IPPT	ECL
SLS-IPPT **SLS**-IPPT*		*Sinterit Lisa* [polyamid powder]	IPPT	ECL
DMLS-IPPT **DMLS**-IPPT*		*EOS EOSINT M280* [aluminium powder]	IPPT	ECL
LCD-IPPT		*Zortrax Inkspire* [photopolymer resin]	IPPT	
FDM-UTC		*Makerbot Replicator Z18* [polymer filament ABS]	UTC	
SLS-i-UTC		*3D Systems ProJet 160* [polyamid powder] (impregnated)	UTC	ECL
SLA-UTC **SLA**-UTC*		*Formlabs Form 2* [photopolymer resin]	UTC	ECL
DLP-EMPA		*Kudo3D Titan 1* [photopolymer resin]	EMPA	
DLP-MIT DLP-MIT*	⌀ **30 mm**	*Autodesk Ember* [photopolymer resin]	MIT	LAUM
LCD-TCD	⌀ **40 mm**	*Anycubic Photon* [photopolymer resin]	TCD	
SLA-TCD		*Formlabs Form 2* [photopolymer resin]	TCD	
SLM-TCD		*3D Systems ProX* [cobalt-chromium powder]	TCD	
FDM-TCD		*Creality Ender 3* [polymer filament ABS]	TCD	
FDM-TUe*		*Ultimaker 2* [polymer filament ABS]	TUe	KUL

The asterisk symbol "*" means that the result was measured by a laboratory that did not produce the sample.

representative results for most of the samples listed in Table 2 and described in Section 3 will be presented in Section 5, including even some of the results obtained for samples of evidently very poor quality to illustrate the resulting change in the nature of the sound absorption curves.

To facilitate quick identification of measurement results (presented in Section 5) and the corresponding samples the result labels used to denote the measurement curves are collected in Table 3 together with the corresponding tube (sample) diameter, AM device, material, manufacturer, etc. For example, the label "**SLA**-UTC" means that the result denoted in this way was measured in a 29 mm impedance

tube for a resin sample manufactured by UTC in SLA technology using *Formlabs Form 2*, and the sample was tested by its manufacturer. A slightly modified label "**SLA**-UTC* " means that the result for this sample was measured by ECL, that is, a laboratory which did not produce the sample, but simply got it for independent testing from UTC. The sample micro-geometry (i.e. OPC-3, OPC-5, FPC-X, FPC-Y, or FPC-Z) is specified on each graph which compares the results obtained for samples with the same micro-geometry (and height). The only exception is the graphs in Figure 20 where sound absorption for samples with different cell orientation are compared, and the curve labels are complemented by a micro-geometry reference.

5. Measurement results

5.1. Sound absorption for OPC samples

Sound absorption measured for OPC-3 samples that were produced using six different AM technologies (viz.: FDM/FFF, SLS, DMLS, LCD, SLA, and DLP) and various devices are compared in Figure 15. Recall that the size of the cubic periodic cell in these samples is 3 mm, while their height is 36 mm. However, instead of being only backed by the rigid wall, the samples were also tested with an air gap of 20 mm or 40 mm set between the sample and the rigid plunger closing the impedance tube. Representative results for some of the samples backed with such air cavities are presented in Figures 15(b), and 15(c), respectively.

Similarly, the results of acoustic absorption for OPC-5 samples (cell size: 5 mm, height: 60 mm) manufactured using various 3D printing devices are also compared for the mentioned configuration cases, i.e.: without air gap, or backed with an air gap of 20 mm or 40 mm (see Figure 16).

The results presented in Figures 15 and 16 (see also Table 3 to decode the result labels) were measured in impedance tubes of two different sizes, namely, with a diameter of 29 mm and 30 mm. In the latter case, it was the samples manufactured by MIT in DLP technology and tested by MIT and also (independently) by LAUM. On the graphs we present the absorption curves obtained by LAUM according to the ISO standard [35]. They were virtually the same (though less fuzzy) as the curves provided by the manufacturer of samples who measured them according to the ASTM standard [36]. The absorption curves measured in 29 mm impedance tubes by IPPT and UTC (i.e. the manufacturers of samples) were very well confirmed with independent tests by ECL. Although the samples were measured in different laboratories at slightly different conditions of pressure, temperature and humidity, discrepancies were very small indeed, and here we present only the curves obtained by the manufacturers.

A very good agreement is found between all curves measured for OPC-5 samples and between almost all curves measured for OPC-3 samples. The frequencies of absorption peaks are consistent across all OPC-5 samples and the main discrepancies are in wide frequency ranges between the peaks where the resin samples (SLA, LCD, and also DLP) have the lowest absorption, which was rather expected since the surface of resin samples is smooth and without fibres or other important imperfections.

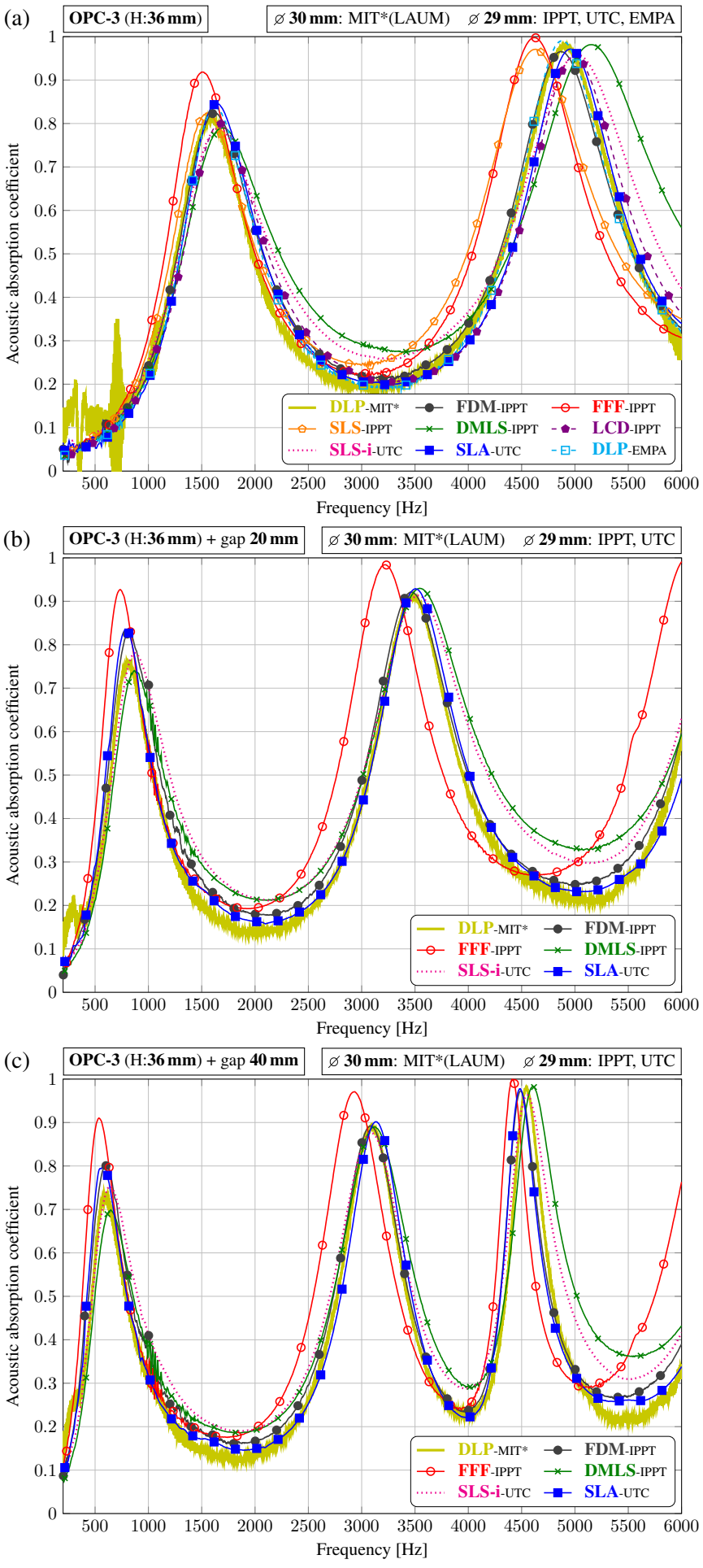

Figure 15: Sound absorption measured for OPC-3 samples: (a) no air gap, (b) with an air gap of 20 mm, (c) with an air gap of 40 mm

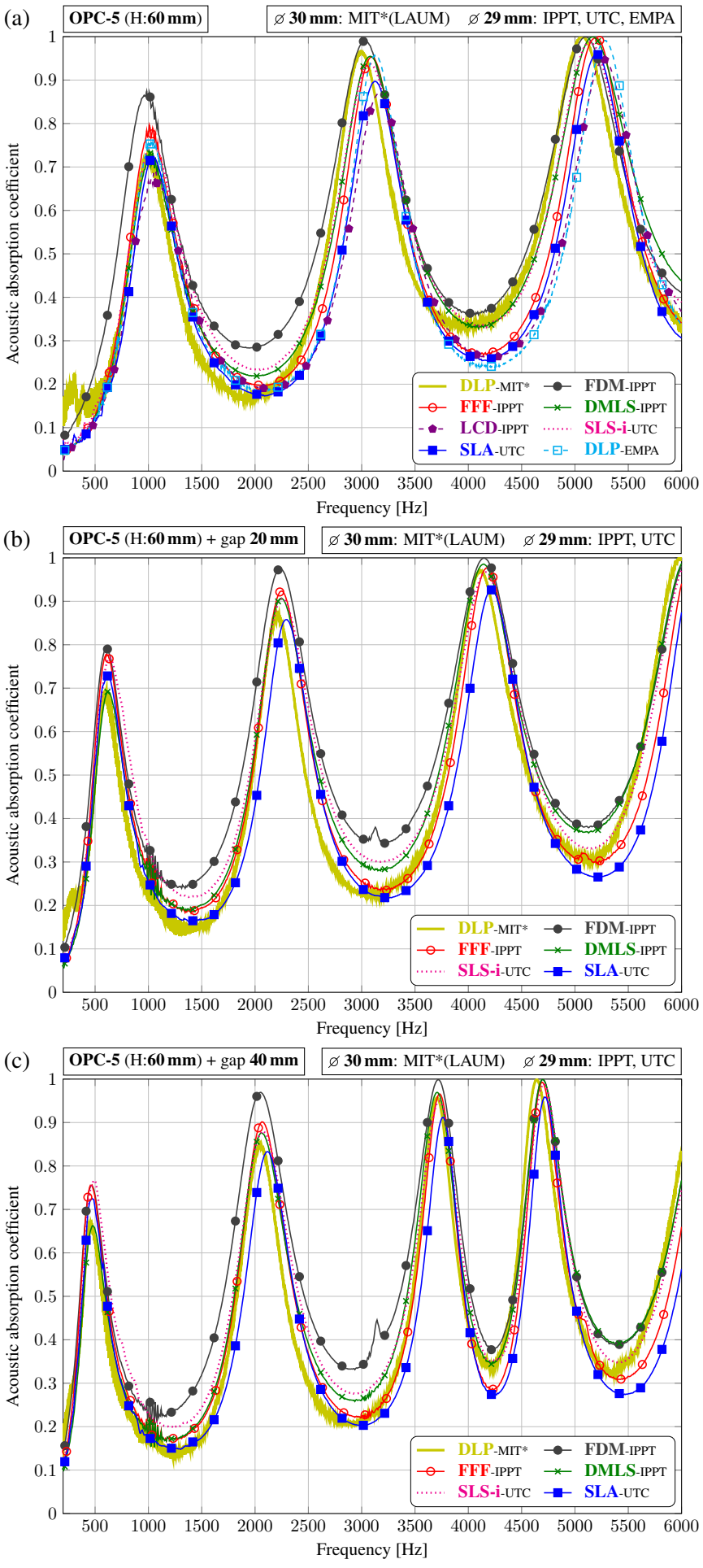

Figure 16: Sound absorption measured for OPC-5 samples: (a) no air gap, (b) with an air gap of 20 mm, (c) with an air gap of 40 mm

5.2. *Sound absorption for FPC samples measured in tubes with a diameter of 29 mm*

Figures 17, 18, and 19 compare sound absorption curves measured in tubes with a diameter of 29 mm for FPC-X, FPC-Y, and FPC-Z samples, respectively. The presented results (see Table 3 to decode the result labels) are obtained for samples (with a periodic cell size of 5 mm, and height of 50 mm) that were manufactured in four substantially different technologies (viz.: FDM/FFF, SLS, DMLS, and SLA) using various devices available in three laboratories (IPPT, UTC, and EMPA). For almost all of these samples, in addition to the standard configuration with a rigid backing, the acoustic absorption was also measured in two additional configuration cases, i.e. when an air gap of 20 mm or 40 mm, respectively, was added between the sample and the rigid end of the impedance tube. Most of these results are also shown in the graphs below. The following observations were made from a comparison of the corresponding absorption curves.

In general, a very good agreement is found between the absorption curves measured for the corresponding SLA samples (manufactured by UTC, and independently by EMPA), SLS samples (manufactured by IPPT), and high-quality FDM/FFF samples (by IPPT). Moreover, for most of these samples, rather unexpectedly, this consistency of measurement results applies throughout almost the whole frequency range considered (i.e. from 200 Hz up to nearly 6 kHz). Only for some of them, more significant discrepancies appear at higher frequencies above 4.5 kHz. This was, in fact, expected for FPC samples because their micro-geometry is more complex than in the case of OPC samples, and is therefore more prone to imperfections during the 3D-printing process. And small inconsistent imperfections in micro-geometry cause differences in measurements at higher frequencies.

A clear difference can be seen at medium and higher frequencies between the SLS samples manufactured by UTC and impregnated with cyanoacrylate, and the non-impregnated SLS samples manufactured by IPPT. Recall that SLS samples produced by UTC were sintered from a larger grain powder, which resulted in microporosity requiring impregnation [37, 38]. For the impregnated samples, medium- and high-frequency absorption peaks are shifted to even higher frequencies. Although this discrepancy was not observed for OPC samples, it can be associated with impregnation in the case of FPC samples.

The absorption curves measured for FPC samples made of metal in DMLS technology are only slightly different from most of the other curves: their second and third absorption peaks are shifted to slightly lower frequencies, and for FPC-Y and FPC-Z samples the curves become rather flat above 4 kHz. To some extent, these discrepancies may also be related to the fact that metal samples are wrapped with tape (to avoid scratching the tube).

In Figures 17(a), 18(a), and 19(a), we also intentionally show the results obtained for a poor quality FDM sample produced using *Makerbot Replicator Z18* from an ABS material suitable for printing shapes with not so small details. Even for these samples, the first absorption peaks (which appear below 1 kHz for FPC samples) are very well represented. On the other hand, the second and third absorption peaks are shifted to significantly higher frequencies, and the total absorption between the peaks is increased in

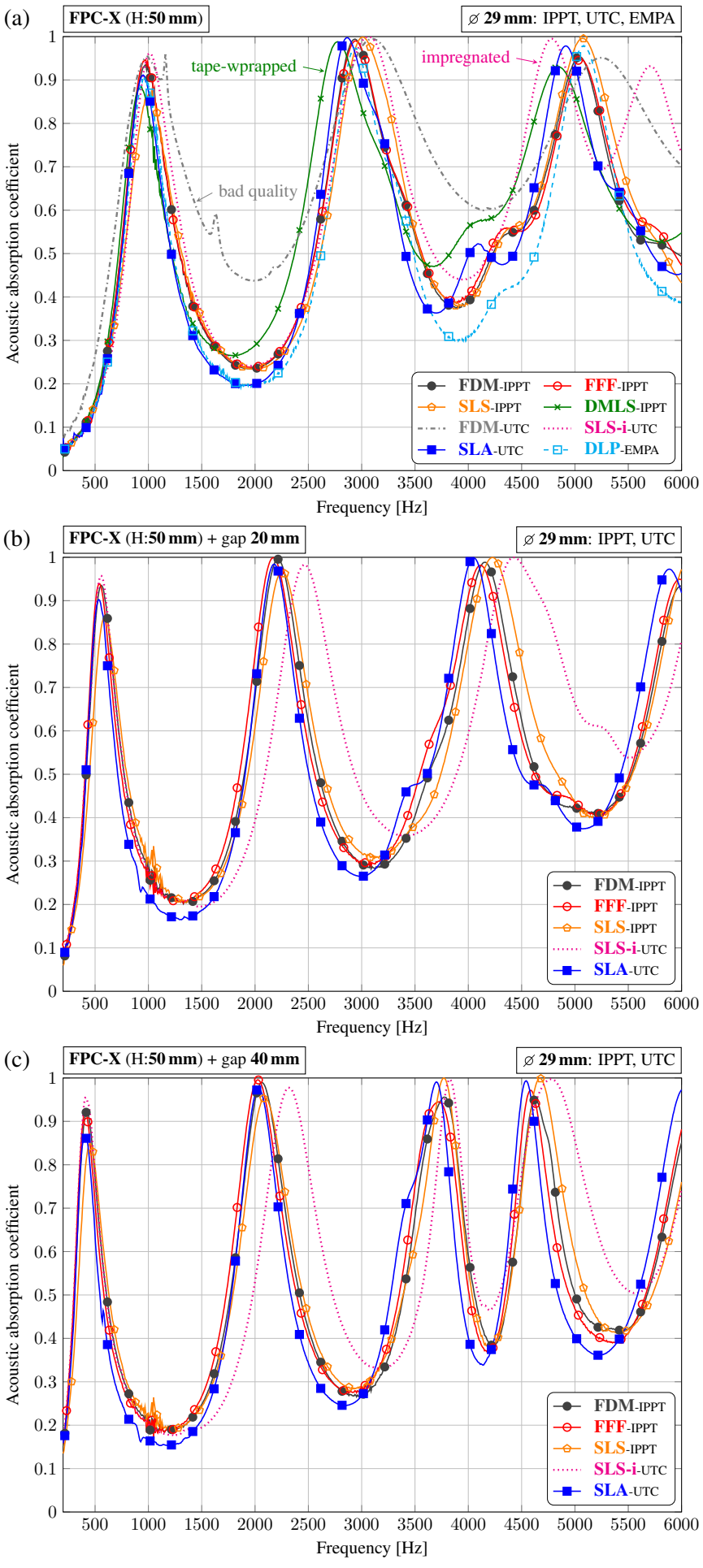

Figure 17: Sound absorption measured for FPC-X samples: (a) no air gap, (b) with an air gap of 20 mm, (c) with an air gap of 40 mm

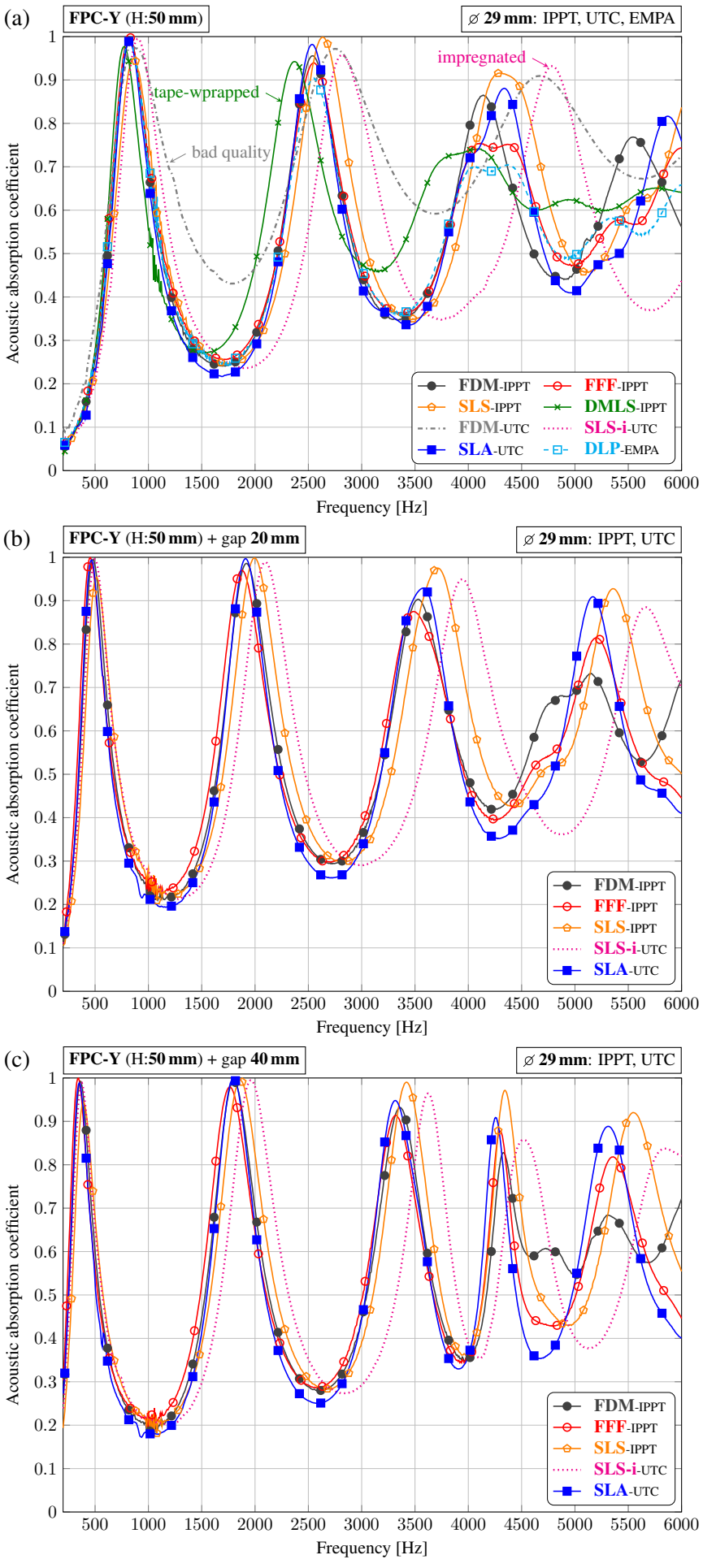

Figure 18: Sound absorption measured for FPC-Y samples: (a) no air gap, (b) with an air gap of 20 mm, (c) with an air gap of 40 mm

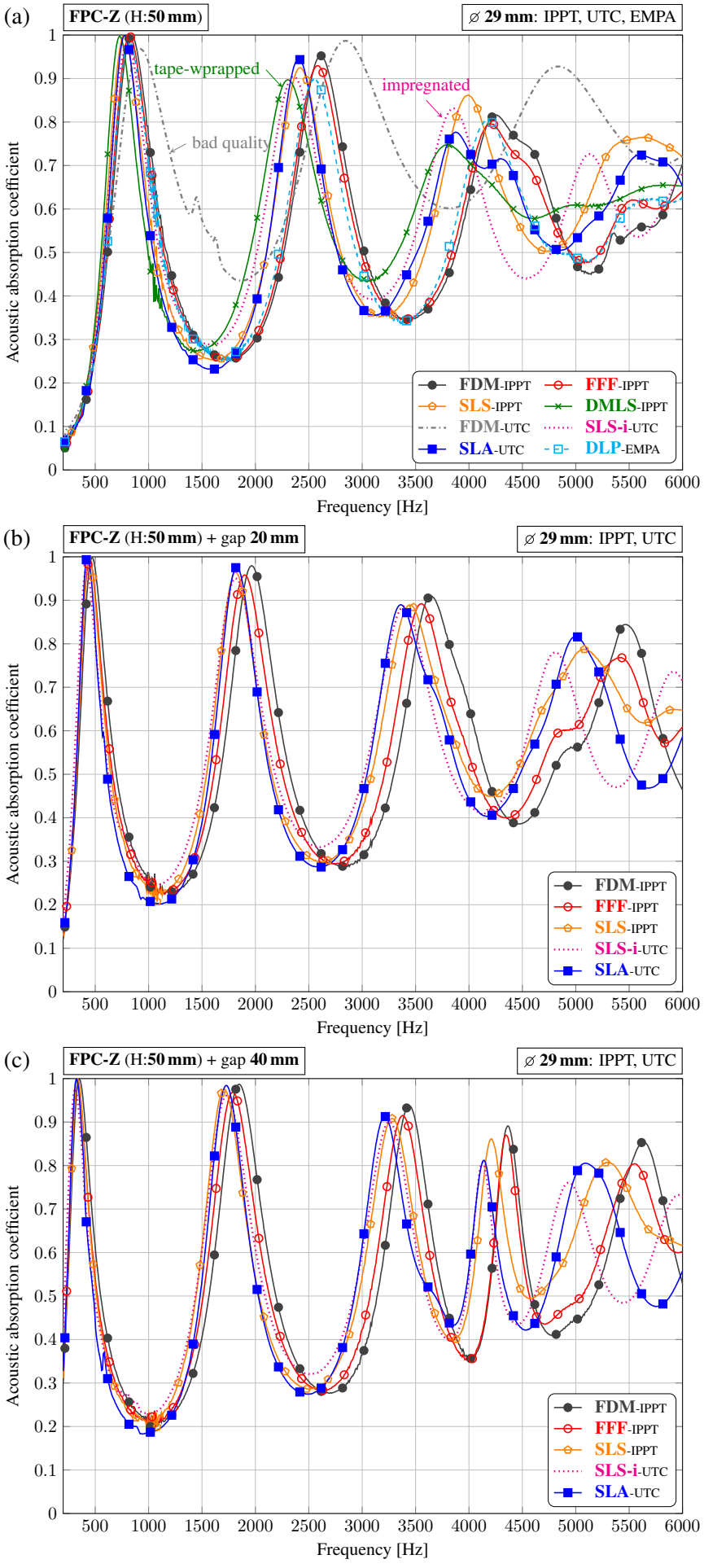

Figure 19: Sound absorption measured for FPC-Z samples: (a) no air gap, (b) with an air gap of 20 mm, (c) with an air gap of 40 mm

the case of these FDM samples. All this is caused by imperfections (surface roughness, smaller pore and channel sizes, fibres inside the pores and across the channels) visible in enlarged photographs of these samples shown in Figure 7.

Finally, in Figure 20, again we present the results for FPC samples manufactured by UTC in SLA technology and by IPPT in SLS technology, this time to directly compare sound absorption by samples with different FPC orientation. It can now be clearly seen that the curves obtained for the FPC-Y and FPC-Z samples are quite similar in nature compared to the FPC-X curve (in particular, their absorption peaks are shifted to relatively lower frequencies). Both graphs in Figure 20 show, in fact, three pairs of absorption curves, that is, two measurements for each of the three types of FPC sample (viz., orientation

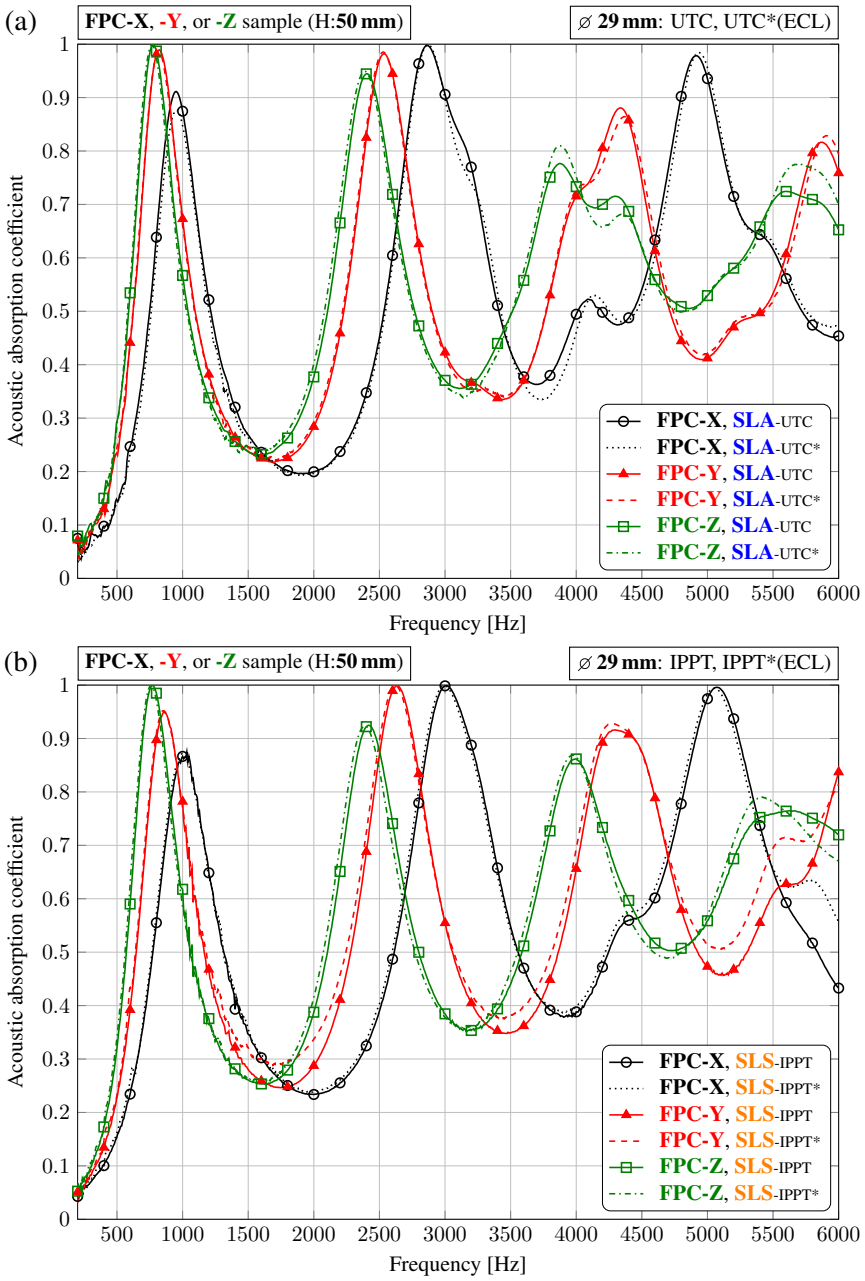

Figure 20: Sound absorption measured for FPC samples: (a) manufactured by UTC in SLA technology, (b) manufactured by IPPT in SLS technology. Two results are shown for each sample: one measured by the sample manufacturer and the other by ECL

FPC-X, FPC-Y, and FPC-Z). The first measurement in each pair is from the sample manufacturer (i.e. UTC or IPPT), while the second result was measured by ECL. It is easy to see that the differences between the measurements in each pair are insignificant and actually similar to the differences that usually occur when repeating acoustic tests for the same sample (in the same laboratory).

5.3. Sound absorption for FPC samples measured in tubes with different diameters

In Figure 21, acoustic absorption curves measured in 40 mm impedance tubes for FPC samples manufactured by TCD in FDM, SLM, SLA, and LCD technologies, and also for samples manufactured by TUe in FDM technology, are compared with each other and with the corresponding results measured in 30 mm tubes for FPC samples manufactured by MIT in DLP technology. In addition, several absorption curves measured in 29 mm impedance tubes for FPC samples manufactured by UTC in SLA technology and by IPPT in DMLS technology, and already shown in Section 5.2, are again plotted as reference in the relevant graphs in Figure 21, in the frequency range up to 4.5 kHz (valid for 40 mm impedance tubes). To decode the labels for specific results, see Table 3.

The general observation is that the discrepancy between the measurements of the corresponding 40 mm samples is greater than for most of the samples manufactured for tubes with a diameter of 29 mm. Also for 40 mm samples these discrepancies are already growing above 3.5 kHz. There are several reasons for this.

The quality of 40 mm FDM samples manufactured by TUe (and acoustically tested by KUL) is lower than that of the 29 mm FDM samples manufactured by IPPT using *Flashforge Creator PRO* or *Zortrax M200* (though it is better than the quality of samples 3D-printed with *Makerbot Replicator Z18*). LCD samples are also of rather poor quality because some of the channels are clogged with resin that was not completely removed. Nevertheless, the agreement for the remaining resin samples (i.e. excluding the LCD ones) is rather good, as it is in the case of FDM samples produced by TCD. It should also be noted that the absorption curves for 30 mm DLP samples are very similar to the sound absorption measured for 29 mm metal samples wrapped in tape.

5.4. Surface acoustic impedance for some of the FPC samples

Figures 22–24 show the real and imaginary parts of the (normalised) surface acoustic impedance measured for some FPC samples. The surface acoustic impedance shown on the graphs is normalised, i.e. divided by the characteristic air impedance accurately determined during the acoustic tests on the basis of ambient mean pressure, temperature, and humidity conditions.

The impedance curves were measured in 29 mm tubes by sample manufacturers and independently by ECL. In fact, they were used to calculate the corresponding sound absorption curves, which are presented in Section 5.2. One may notice that the poles (zeroes) of the imaginary part of the surface impedance correspond to the extrema (local minima and maxima) of its real part and to the extrema (but this time local maxima and minima, respectively) of the corresponding absorption curve. We present

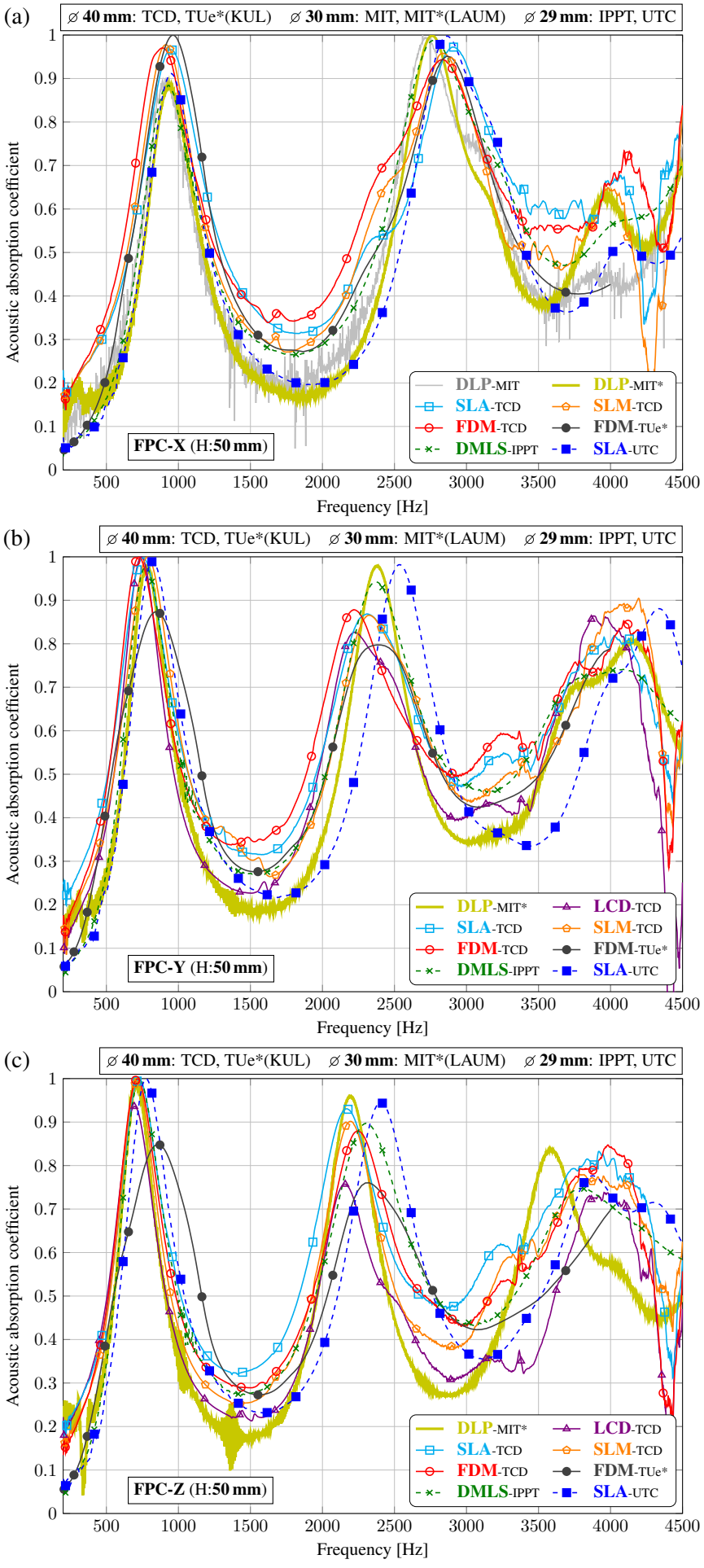

Figure 21: Sound absorption measured in tubes with different diameters for: (a) FPC-X samples, (b) FPC-Y samples, (c) FPC-Z samples

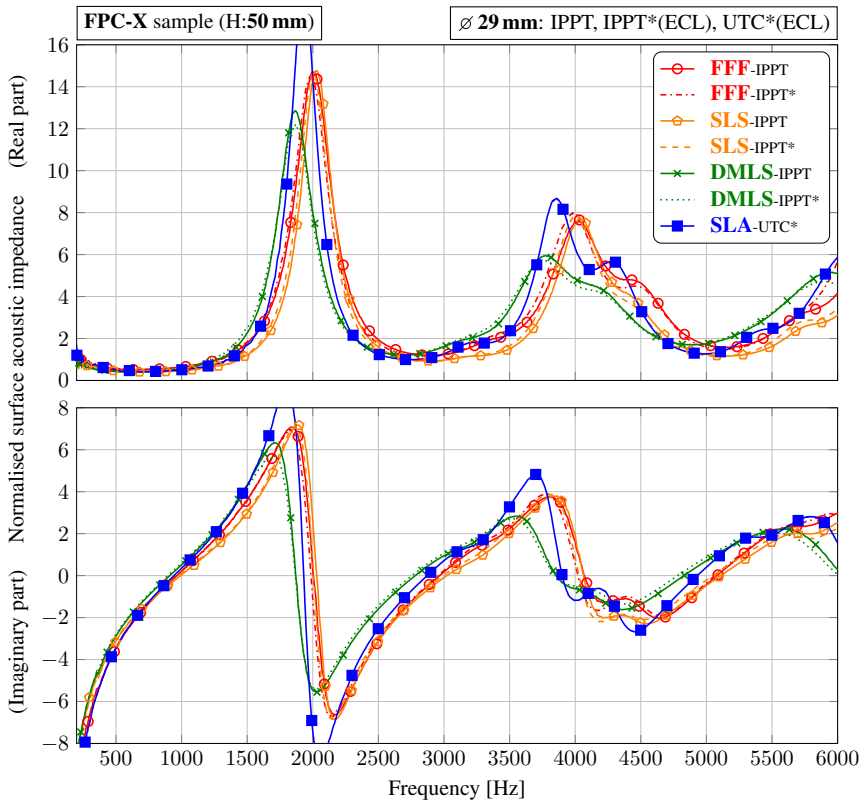

Figure 22: Normalised surface acoustic impedance independently measured by ECL and IPPT for some FPC-X samples manufactured by IPPT and UTC

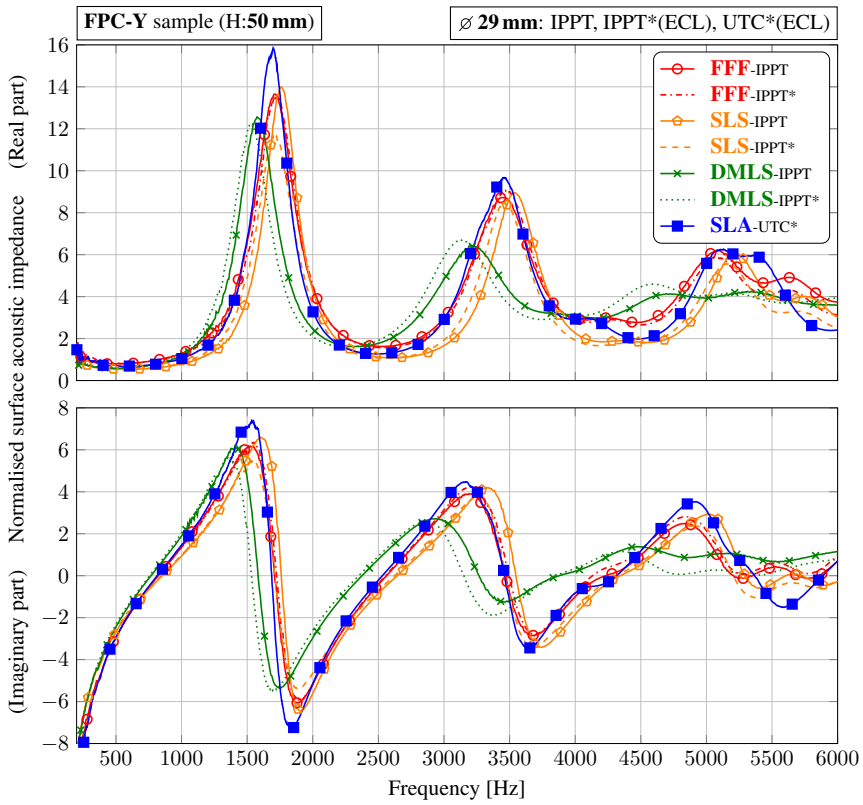

Figure 23: Normalised surface acoustic impedance independently measured by ECL and IPPT for some FPC-Y samples manufactured by IPPT and UTC

these impedance curves because they can be useful when looking for discrepancies, since in absorption curves some of the measured information is “compacted”. The impedance curves measured for different

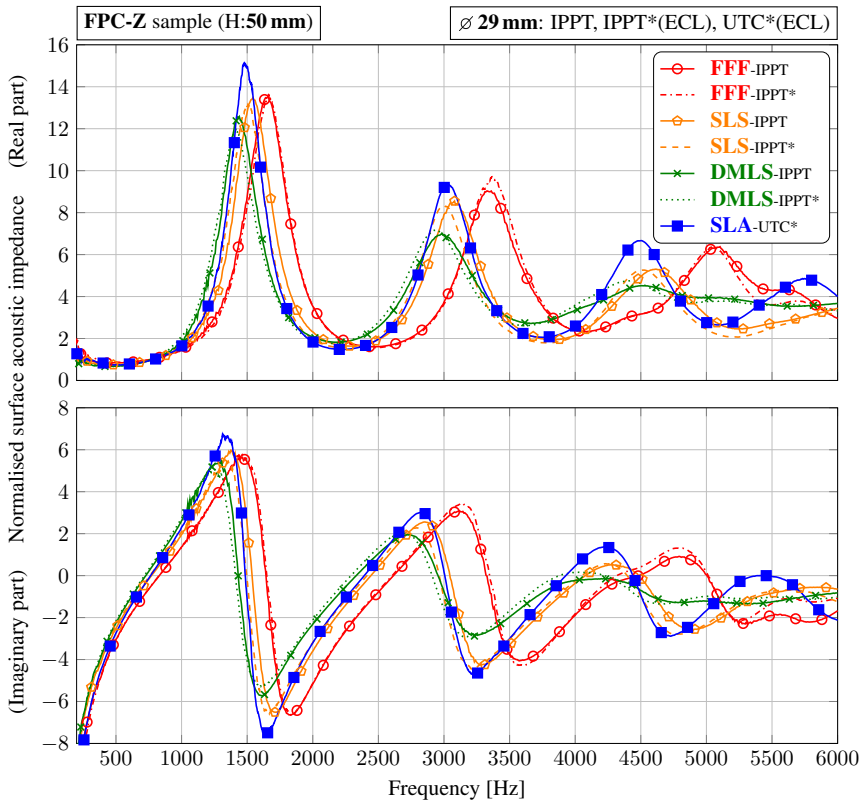

Figure 24: Normalised surface acoustic impedance independently measured by ECL and IPPT for some FPC-Z samples manufactured by IPPT and UTC

samples of the same (macro- and) micro-geometry are still very similar but perhaps with more noticeable discrepancies. Finally, it should be noted again that the results measured by IPPT and ECL for the same sample are practically the same or very similar, although the tests were carried out in different laboratories over a period of several months (in early springtime by IPPT, and in summertime by ECL).

6. Concluding remarks

Based on the examination of samples and comparison of measured sound absorption curves and surface acoustic impedance, we determined that there are three reasons for the discrepancy between the measurement results:

1. Overall manufacturing quality associated with AM technology and the material used for production. The main factor here is the correct (undistorted) reproduction of the designed micro-geometry related to the resolution of 3D-printing (however, it should be remembered that the pore and channel diameters will always be slightly different than in the case of the CAD models used for 3D-printing). Other factors are small imperfections (fibres, completely or partially clogged channels, microporosity, etc.) that appear during the production process, but also in post-production treatment (due to difficulties in removing resin or powder, deformation during curing, problems with curing inner parts of resin porous samples), and sometimes even later (delayed shrinkage effect).
2. Matching samples to the diameter of the impedance tube. This is a well-known reason for possible discrepancies [21, 39]. When 3D printing samples for the impedance tube, one should proceed

with caution as follows (to get a 'perfect' or exact fit, tight or only acceptable): (a) samples are 3D-printed with slightly larger diameters than the diameter of the tube, and then cut to fit ('*perfect*', *exact*, or *tight* fit depending on the cutting method); (b) diameter is determined by trial and error (for specific AM device and material), so the samples can be 3D-printed for a very tight fit (rather *tight* than *exact*, but can be sufficient if the cylindrical shape of the samples is not distorted); (c) samples are 3D-printed with a slightly smaller diameter than the tube, and then wrapped with tape (acceptable, but should be avoided if possible).

3. The proposed periodic micro-geometries have relatively large features (i.e. large pores, wide channels), so the sample faces have large details around their circular edges, different for different sample diameters, because they depend on how the periodic cells are cut by the cylinder edge. This can affect the measurements.

Nevertheless, the overall consistency of the results measured for all good quality samples with the same periodic microstructure proved to be good and we can also recommend SLA technology as the most suitable for manufacturing samples. On the other hand, the presented results show that for such relatively large periodic microstructures sufficient quality is achievable even when using FDM technology, provided that one has some experience (or luck) in matching the selection of parameters and materials for 3D-printing.

Imperfections (roughness, small fibers inside voids, microporosity) tend to significantly increase sound absorption, which is usually desirable. We believe that this can also be used to assess the 3D printing quality using acoustic measurements, like it was done, e.g., in [40]. It should be noted that, for example, the sound absorption between the peaks is very low, even at higher frequencies for samples with smooth surfaces without noticeable imperfections.

Acknowledgements

This work is based upon collaboration between the authors supported by European Cooperation in Science and Technology (COST) through the COST Action CA15125 – DENORMS: "*Designs for Noise Reducing Materials and Structures*". T. G. Zieliński and K. C. Opiela would also like to acknowledge the financial support from the National Science Centre (NCN), Poland, under Grant Agreement No. 2015/19/B/ST8/03979. The research of A. Carvalho de Sousa is funded by an Early Stage Researcher grant within the European Project ACOUTECT Marie Curie Initial Training Network (GA 721536). The research of E. Deckers is funded by a postdoctoral grant from the Research Foundation – Flanders (FWO).

References

[1] J. F. Allard, N. Atalla, Propagation of Sound in Porous Media: Modeling Sound Absorbing Materials, 2nd ed., John Wiley & Sons, Chichester, 2009.

[2] J. Boulvert, T. Cavalieri, J. Costa-Baptista, L. Schwan, V. Romero-García, G. Gabard, E. R. Fotsing, A. Ross, J. Mardjono, J.-P. Groby, Optimally graded porous material for broadband perfect absorption of sound, J. Appl. Phys. 126 (2019) 175101.

[3] K. Attenborough, Microstructures for lowering the quarter wavelength resonance frequency of a hard-backed rigid-porous layer, Appl. Acoust. 130 (2018) 188–194.

[4] K. Attenborough, Macro- and micro-structure designs for porous sound absorbers, Appl. Acoust. 145 (2019) 349–357.

[5] I. Gibson, D. Rosen, B. Stucker, Additive manufacturing technologies: 3D printing, rapid prototyping, and direct digital manufacturing, 2nd Edition, Springer-Verlag, New York, 2015.

[6] S. Kumar, A. K. S. Choudhary, A. K. Singh, A. K. Gupta, A comparison of additive manufacturing technologies, International Journal for Innovative Research in Science & Technology 3 (2016) 147–152.

[7] T. D. Ngo, A. Kashani, G. Imbalzano, K. T. Nguyen, D. Hui, Additive manufacturing (3D printing): A review of materials, methods, applications and challenges, Compos. Part B-Eng. 143 (2018) 172–196.

[8] X. Wang, M. Jiang, Z. Zhou, J. Gou, D. Hui, 3D printing of polymer matrix composites: A review and prospective, Compos. Part B-Eng. 110 (2017) 442–458.

[9] A. Mitchell, U. Lafont, M. Hołyńska, C. Semprimoschnig, Additive manufacturing - A review of 4D printing and future applications, Addit. Manuf. 24 (2018) 606–626.

[10] O. Diegel, A. Nordin, D. Motte, A practical guide to design for additive manufacturing, 1st Edition, Springer series in advanced manufacturing, Springer, Singapore, 2019.

[11] M. Jiménez, L. Romero, I. A. Domínguez, M. d. M. Espinosa, M. Domínguez, Additive manufacturing technologies: An overview about 3D printing methods and future prospects, Complexity 2019 (2019) 9656938.

[12] ISO 17296-2: Additive manufacturing – General principles – Part 2: Overview of process categories and feedstock (2015).

[13] T. G. Zieliński, Pore-size effects in sound absorbing foams with periodic microstructure: modelling and experimental verification using 3D printed specimens, in: P. Sas, D. Moens, A. van de Walle (Eds.), Proceedings of ISMA2016 International Conference on Noise and Vibration Engineering and USD2016 International Conference on Uncertainty in Structural Dynamics, 2016, pp. 95–104.

[14] K. C. Opiela, T. G. Zieliński, Microstructural design, manufacturing and modelling of an adaptable porous composite sound absorber, Compos. Part B-Eng. 187 (2020) 107833.

[15] H. J. Rice, J. Kennedy, P. Göransson, L. Dowling, D. Trimble, Design of a Kelvin cell acoustic metamaterial, J. Sound Vib. 472 (2020) 115167.

[16] E. R. Fotsing, A. Dubourg, A. Ross, J. Mardjono, Acoustic properties of periodic micro-structures obtained by additive manufacturing, Appl. Acoust. 148 (2019) 322–331.

[17] T. Ring, S. Langer, Design, experimental and numerical characterization of 3D-printed porous absorbers, Materials 12 (2019) 3397.

[18] Z. Liu, J. Zhan, M. Fard, J. Davy, Acoustic properties of multilayer sound absorbers with a 3D printed micro-perforated panel, Appl. Acoust. 121 (2017) 25–32.

[19] Z. Liu, J. Zhan, M. Fard, J. Davy, Acoustic measurement of a 3D printed micro-perforated panel combined with a porous material, Measurement 104 (2017) 233–236.

[20] T. G. Zieliński, F. Chevillotte, E. Deckers, Sound absorption of plates with micro-slits backed with air cavities: Analytical estimations, numerical calculations and experimental validations, Appl. Acoust. 146 (2019) 261–279.

[21] K. V. Horoshenkov, A. Khan, F.-X. Bécot, L. Jaouen, F. Sgard, A. Renault, N. Amirouche, F. Pompoli, N. Prodi, P. Bonfiglio, G. Pispola, F. Asdrubali, J. Hübelt, N. Atalla, C. K. Amédin, W. Lauriks, L. Boeckx, Reproducibility experiments on measuring acoustical properties of rigid-frame porous media (round-robin tests), J. Acoust. Soc. Am. 122 (2007) 345–353.

[22] P. Bonfiglio, F. Pompoli, K. V. Horoshenkov, M. I. B. S. A. Rahim, L. Jaouen, J. Rodenas, F.-X. Bécot, E. Gourdon, D. Jaeger, V. Kursch, M. Tarello, N. B. Roozen, C. Glorieux, F. Ferrian, P. Leroy, F. B. Vangosa, N. Dauchez, F. Foucart, L. Lei, K. Carillo, O. Doutres, F. Sgard, R. Panneton, K. Verdiere, C. Bertolini, R. Bär, J.-P. Groby, A. Geslain, N. Poulain, L. Rouleau, A. Guinault, H. Ahmadi, C. Forge, How reproducible are methods to measure the dynamic viscoelastic properties of poroelastic media?, J. Sound Vib. 428 (2018) 26–43.

[23] A. du Plessis, S. G. le Roux, Standardized X-ray tomography testing of additively manufactured parts: A round robin test, Addit. Manuf. 24 (2018) 125–136.

[24] A. Townsend, R. Racasan, R. Leach, N. Senin, A. Thompson, A. Ramsey, D. Bate, P. Woolliams, S. Brown, L. Blunt, An interlaboratory comparison of X-ray computed tomography measurement for texture and dimensional characterisation of additively manufactured parts, Addit. Manuf. 23 (2018) 422–432.

[25] A. du Plessis, S. G. le Roux, J. Waller, P. Sperling, N. Achilles, A. Beerlink, J.-F. Métayer, M. Sinico, G. Probst, W. Dewulf, F. Bittner, H.-J. Endres, M. Willner, Á. Drégelyi-Kiss, T. Zikmund, J. Laznovsky, J. Kaiser, P. Pinter, S. Dietrich, E. Lopez, O. Fitzek, P. Konrad, Laboratory X-ray tomography for metal additive manufacturing: Round robin test, Addit. Manuf. 30 (2019) 100837.

[26] J. Kennedy, L. Flanagan, L. Dowling, G. J. Bennett, H. Rice, D. Trimble, The influence of additive manufacturing processes on the performance of a periodic acoustic metamaterial, Int. J. Polym. Sci. 2019 (2019) 7029143.

[27] T. G. Zieliński, K. C. Opiela, P. Pawłowski, N. Dauchez, T. Boutin, J. Kennedy, D. Trimble, H. Rice, Differences in sound absorption of samples with periodic porosity produced using various Additive Manufacturing Technologies, in: M. Ochmann, M. Vorländer, J. Fels (Eds.), Proceedings of the 23rd International Congress on Acoustics integrating 4th EAA Euroregio 2019, 2019, pp. 1216–1223.

[28] J.-P. Dalmont, Acoustic impedance measurement, Part I: A review, J. Sound Vib. 243 (2001) 427–439.

[29] J.-P. Dalmont, Acoustic impedance measurement, Part II: A new calibration method, J. Sound Vib. 243 (2001) 441–459.

[30] R. Boonen, P. Sas, W. Desmet, W. Lauriks, G. Vermeir, Calibration of the two microphone transfer function method with hard wall impedance measurements at different reference sections, Mech. Syst. Sig. Process. 23 (2009) 1662–1671.

[31] T. G. Zieliński, Generation of random microstructures and prediction of sound velocity and absorption for open foams with spherical pores, J. Acoust. Soc. Am. 137 (2015) 1790–1801.

[32] J. A. García Galicia, B. Benes, Improving printing orientation for Fused Deposition Modeling printers by analyzing connected components, Addit. Manuf. 22 (2018) 720–728.

[33] L. Yang, K. Hsu, B. Baughman, D. Godfrey, F. Medina, M. Menon, S. Wiener, Additive manufacturing of metals: The technology, materials, design and production, 1st Edition, Springer Series in Advanced Manufacturing, Springer International Publishing, 2017.

[34] L. Dowling, J. Kennedy, S. O'Shaughnessy, D. Trimble, A review of critical repeatability and reproducibility issues in powder bed fusion, Mater. Design 186 (2020) 108346.

[35] ISO 10534-2: Determination of sound absorption coefficient and impedance in impedance tubes (1998).

[36] ASTM E1050-19: standard test method for impedance and absorption of acoustical materials using a tube, two microphones and a digital frequency analysis system (2019).

[37] A. du Plessis, Effects of process parameters on porosity in laser powder bed fusion revealed by X-ray tomography, Addit. Manuf. 30 (2019) 100871.

[38] R. J. Williams, A. Piglione, T. Rønneberg, C. Jones, M.-S. Pham, C. M. Davies, P. A. Hooper, In situ thermography for laser powder bed fusion: Effects of layer temperature on porosity, microstructure and mechanical properties, Addit. Manuf. 30 (2019) 100880.

[39] A. Cummings, Impedance tube measurements on porous media: The effects of air-gaps around the sample, J. Sound Vib. 151 (1991) 63–75.

[40] Y. Ibrahim, Z. Li, C. M. Davies, C. Maharaj, J. P. Dear, P. A. Hooper, Acoustic resonance testing of additive manufactured lattice structures, Addit. Manuf. 24 (2018) 566–576.

[41] OpenSCAD – The Programmers Solid 3D CAD Modeller.
https://www.openscad.org/
(Last viewed 18/02/2020).

[42] OpenSCAD Language.
https://en.wikibooks.org/wiki/OpenSCAD_User_Manual/The_OpenSCAD_Language
(Last viewed 18/02/2020).

[43] FreeCAD – Open-source 3D parametric CAD modeler.
https://www.freecadweb.org/
(Last viewed 18/02/2020).

[44] Import OpenSCAD code (in FreeCAD).
https://www.freecadweb.org/wiki/Import_OpenSCAD_code
(Last viewed 18/02/2020).

Appendix A. Code listings for the CAD models of OPC and FPC samples

Table A.1 contains the code for the CAD models of OPC samples. The code for the CAD models of FPC samples is given in Tables A.2 and A.3. These codes were provided to all laboratories that independently used them to generate STL files and G-codes for their 3D printers. They are in the *OpenSCAD* language [41, 42] and we strongly recommend to use them with *FreeCAD* [43, 44].

Table A.1: *OpenSCAD* code for periodic samples based on OPC

```
// One-Pore-Cell periodic porous sample
// (2019) T.G.Zielinski

// Sizes of periodic elements
Lc = 5;       // cubic cell size [mm]
Dp = 0.9*Lc;  // pore diameter
Dw = 0.4*Lc;  // window diameter

// Sample (and cell array) dimensions
Ds = 29;                        // sample diameter [mm]
Nx = 2*ceil(0.5*ceil(Ds/Lc));  // Nx is even and Nx*Lc >= Ds
Ny = Nx;
Nz = 12;                        // numebr of cell layers
Hs = Nz*Lc;                     // sample height

// Flat-faces parameter (1 or 0)
FFP = 0;

// Auxiliary shifts
Xsh = -0.5*(Nx+1)*Lc;
Ysh = -0.5*(Ny+1)*Lc;
Zsh = -0.5*Lc*FFP;

// Periodic cell
module PeriodicCell(Nfacets=16) {
    difference() {
        cube(size=Lc, center=true);
        sphere(d=Dp, $fn=Nfacets);
        cylinder(h=Lc, d=Dw,  $fn=Nfacets, center=true);
        rotate(a=90, v=[1,0,0])
            cylinder(h=Lc, d=Dw, $fn=Nfacets, center=true);
        rotate(a=90, v=[0,1,0])
            cylinder(h=Lc, d=Dw, $fn=Nfacets, center=true);
    }
}

// PeriodicCell(32);  // Use 0 facets for FreeCAD, 32 for OpenSCAD.
// To generate only a single periodic cell uncomment the line above
// and delete (or comment) all the lines below.

// Cylindrical sample
intersection() {
    cylinder(d=Ds, h=Hs, $fn=128);
    for (nx=[1:1:Nx], ny=[1:1:Ny], nz=[FFP:1:Nz]) {
        translate([nx*Lc+Xsh, ny*Lc+Ysh, nz*Lc+Zsh])
            PeriodicCell(0);  // Use 0 facets for FreeCAD.
    }
}
```

Table A.2: *OpenSCAD* code for periodic samples based on FPC

```
// Four-Pore-Cell periodic porous sample
// (2019) T.G.Zielinski

// PERIODIC POROUS CELL
// Cell size and orientation (rotation)
Lc = 5;         // cubic cell size [mm]
XYorZ = "Z";    // orientation (set "X", "Y", or "Z")
// Rotation axis and angle
RotAxis  = (XYorZ=="X") ? [0,1,0] : (XYorZ=="Y") ? [1,0,0] : [0,0,1];
RotAngle = (XYorZ=="Z") ? 0 : 90;

// Pore size scaling factor
PSSF = 0.9;

// Normalised data for pores (initial diameters + positions)
// Pore 1
d1 = 0.59;                                  // (initial diameter)
x1 = 0.00;    y1 = 0.00;    z1 = 0.00;      // (coordinates)
p1 = [x1,y1,z1];                            // (position)

// Pore 2
d2 = 0.64;                                  // (initial diameter)
x2 = -0.47;   y2 = -0.44;   z2 = 0.04;      // (coordinates)
p2 = [x2,y2,z2];                            // (position)

// Pore 3
d3 = 0.67;                                  // (initial diameter)
x3 = 0.45;    y3 = -0.05;   z3 = -0.35;     // (coordinates)
p3 = [x3,y3,z3];                            // (position)

// Pore 4
d4 = 0.76;                                  // (initial diameter)
x4 = 0.04;    y4 = -0.51;   z4 = 0.37;      // (coordinates)
p4 = [x4,y4,z4];                            // (position)

pos = [
    [p1, [0, 0, 0]],
    [p2, [0, 0, 0], [ 1, 0, 0], [0, 1, 0], [ 1, 1, 0]],
    [p3, [0, 0, 0], [-1, 0, 0], [0, 0, 1], [-1, 0, 1]],
    [p4, [0, 0, 0], [ 0, 1, 0], [0, 0,-1], [ 0, 1,-1]],
];

Diameters = [d1, d2,d2,d2,d2, d3,d3,d3,d3, d4,d4,d4,d4];
Positions = Fun1(len(pos),pos);

function Fun1(n,X) =
    ( n==0 ? [] : concat(Fun1(n-1,X), Fun2(len(X[n-1])-1,X[n-1])) );

function Fun2(n,X) =
    ( n==0 ? [] : concat(Fun2(n-1,X), [X[0]+X[n]]) );

// Window diameter between two pores (NaN for non-overlapping pores)
function WindowDiameter(P1, D1, P2, D2) =
    let(
    R1R1 = 0.25*D1*D1,  R2R2 = 0.25*D2*D2,
    dd = pow(norm(P1-P2),2),
    xi = ( dd + R1R1 - R2R2 )/(2*dd)
    )
    2*sqrt( R1R1 - xi*xi*dd );

// To be continued in the next Listing ...
```

Table A.3: Continuation of the code from Table A.2

```
// ... continuation of the previous Listing.

// Cylinder between two points
module CylinderBetweenPoints(P1, P2, D, Nfacets=16) {
    PP = P2-P1;  x = PP[0];  y = PP[1];  z = PP[2];
    height = norm(PP);       // cylinder height
    beta = acos(z/height);   // inclination angle
    gamma = atan2(y,x);      // azimuthal angle
    translate(P1){
        rotate([0, beta, gamma])
            cylinder(h=height, d=D, $fn=Nfacets);
    }
}

// Periodic cell (skeleton)
module PeriodicCell(Nfacets=16) {
    rotate(a=RotAngle, v=RotAxis)
    difference() {
        cube(size=Lc, center=true);
        union() {
            N = len(Diameters)-1;
            for(m = [0:1:N]) {
                Pm = Positions[m];
                Dm = Diameters[m];
                dm = round(PSSF*100*Dm)/100;
                translate(Pm*Lc) sphere(d=dm*Lc, $fn=Nfacets);
                for(n = [(m+1):1:N]) {
                    Pn = Positions[n];
                    Dn = Diameters[n];
                    Dw = WindowDiameter(Pm, Dm, Pn, Dn);
                    if(Dw>0) {
                        dw = round(100*Dw)/100;
                        CylinderBetweenPoints(Pm*Lc, Pn*Lc, dw*Lc, Nfacets);
                    }
                }
            }
        }
    }
}

// PeriodicCell(32);  // Use 0 facets for FreeCAD, 32 for OpenSCAD.
// To generate only a single periodic cell uncomment the line above
// and delete (or comment) all the lines below.

// CYLINDRICAL PERIODIC POROUS SAMPLE
// Sample (and cell array) dimensions
Ds = 29;                        // sample diameter [mm]
Nx = 2*ceil(0.5*ceil(Ds/Lc));  // Nx is even and Nx*Lc >= Ds
Ny = Nx;
Nz = 10;                        // numebr of cell layers
Hs = Nz*Lc;                     // sample height

// Cylindrical sample
nNx = [-0.5*(Nx-1) : 1 : 0.5*(Nx-1)];
nNy = [-0.5*(Ny-1) : 1 : 0.5*(Ny-1)];
nNz = [0.5 : 1 : (Nz-0.5)];
intersection() {
    cylinder(d=Ds, h=Hs, $fn=128);
    union() {
        for (nx=nNx, ny=nNy, nz=nNz)
            translate([Lc*nx, Lc*ny, Lc*nz])
                PeriodicCell(0);  // Use 0 facets for FreeCAD.
    }
}
```